Spectrochimica Acta Part A: Molecular and Biomolecular Spectroscopy 192 (2018) 343–360

Contents lists available at ScienceDirect

Spectrochimica Acta Part A: Molecular and Biomolecular Spectroscopy

journal homepage: www.elsevier.com/locate/saa

Review Article

Anisotropy (optical, electrical and thermal conductivity) in thin polarizing films for UV/Vis regions of spectrum: Experimental and theoretical investigations

Hooriye Yahyaei [a,*], Siyamak Shahab [b,c,d], Masoome Sheikhi [e], Liudmila Filippovich [c,d], Hora A. Almodarresiyeh [c], Rakesh Kumar [f], Evgenij Dikusar [c], Mostafa Yousefzadeh Borzehandani [g], Radwan Alnajjar [h]

[a] Department of Chemistry, Zanjan Branch, Islamic Azad University, Zanjan, Iran
[b] International Sakharov Environmental University, Department of Biochemistry and Biophysics, 23 Dolgobrodskaya Str., 220009 Minsk, Belarus
[c] Institute of Physical Organic Chemistry, National Academy of Sciences of Belarus,13 Surganov Str., Minsk 220072, Belarus
[d] Institute of Chemistry of New Materials, National Academy of Sciences of Belarus, 36 Skarina Str., Minsk 220141, Belarus
[e] Department of Chemistry, Gorgan Branch, Islamic Azad University, Gorgan, Iran
[f] Department of Chemistry, DAV University, Jalandhar -144012 (Punjab) India
[g] Young Researchers and Elite Club, Rasht Branch, Islamic Azad University, Rasht, Iran
[h] Department of Chemistry, Faculty of Science, University of Benghazi, Benghazi, Libya

ARTICLE INFO

Article history:
Received 29 August 2017
Received in revised form 18 October 2017
Accepted 11 November 2017
Available online 13 November 2017

Keywords:
Polarization
Anisotropy of optical
Electrical and thermal conductivity
PVA matrix
Azomethine dye

ABSTRACT

In the present work, the quantum theoretical calculations of the molecular structures of the three newly synthesized azomethine dyes:

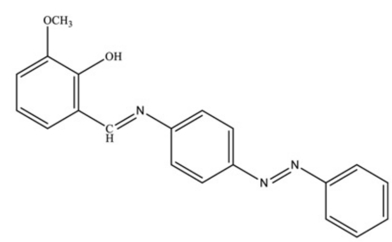

PAZB-3

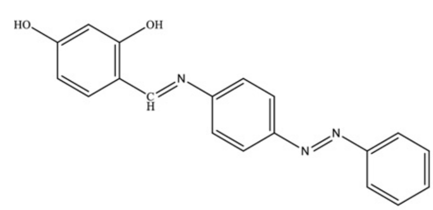

PAZB-11

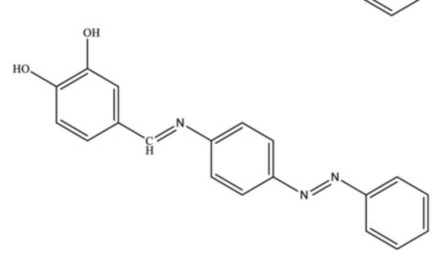

PAZB-12

* Corresponding author.
E-mail addresses: Hooriye_yahyaei@yahoo.com (H. Yahyaei), siyamak.shahab@yahoo.com (S. Shahab), m.sheikhi2@gmail.com (M. Sheikhi), luda1977@list.ru (L. Filippovich), h_al1994@yahoo.com (H.A. Almodarresiyeh), rakesh_nitj@yahoo.co.in (R. Kumar), dikusar@ifoch.bas-net.by (E. Dikusar), jan_1989@ymail.com (M.Y. Borzehandani), radwan.alnajjar@uob.edu.ly (R. Alnajjar).

https://doi.org/10.1016/j.saa.2017.11.029
1386-1425/

have been predicted using Density Functional Theory (DFT) in solvent dimethylformamide (DMF). The geometries of the azomethine dyes were optimized using the PBE1PBE/6-31 + G level of the theory. In addition, the electronic spectra of these compounds in solvent DMF were carried out using the TDPBE1PBE, TDPBEPBE, TDB3LYP methods with 6-31G, 6-31 + G, 6-31 + G*, 6-31 + +G* basis sets. After quantum-chemical calculations three new azomethine dyes for optoelectronic applications were synthesized. Based on polyvinyl alcohol (PVA) and the new synthesized azomethine dyes polarizing films for UV/Vis regions of the spectrum were developed. The main optical parameters of polarizing PVA-films (Transmittance and Polarization Efficiency) have been measured and discussed. Anisotropy of electrical and thermal conductivity of the PVA-films has been investigated.

Contents

1. Introduction

Compounds containing an azo (—N=N—) group are often important organic molecules [1] such as organic dyes [2], initiator in radical reactions [3] indicator factor [4], and therapeutic agents [5]. Also, compounds containing an imine (—C=N—) group have isoelectronic properties and exhibited hole-transporting properties [6]. Azomethines containing both imine (—C=N—) and azo (—N=N—) groups are important compounds in the field of medicinal chemistry [7,8]. Azomethines have many applications, for example, they are used in photoluminescence materials [9], optical materials and devices [10], organic light-emitting diodes [11], photovoltaic cells [12], polarizing films [10,13,14], lasers, spectroscopic analysis, liquid crystal devices and optoelectronic systems [9–14]. In recent years, computational chemistry has become an important tool for chemists and a well-accepted partner for experimental chemistry. HF and DFT are theoretical quantum chemistry methods that have been widely used for the calculation of optimized geometry, absorption spectrum, UV, IR and NMR spectra of the organic compounds [9,15,12–21]. The DFT method in particular, is a major tool in the methodological arsenal of computational organic chemists. Also, Time-Dependent Density Functional Theory (TD-DFT) is used for predicting the absorption spectra of the compounds [13,14]. The new azomethine dye containing hydroxyl (O—H) group, 2-{(E)-[(2-hydroxy-5-methylphenyl)imino]methyl}-4-[(E)-phenyldiazenyl]phenol, has been studied by researchers [22]. They studied thermal properties of the title dye and results indicated that the dye is stable up to 172 °C. In

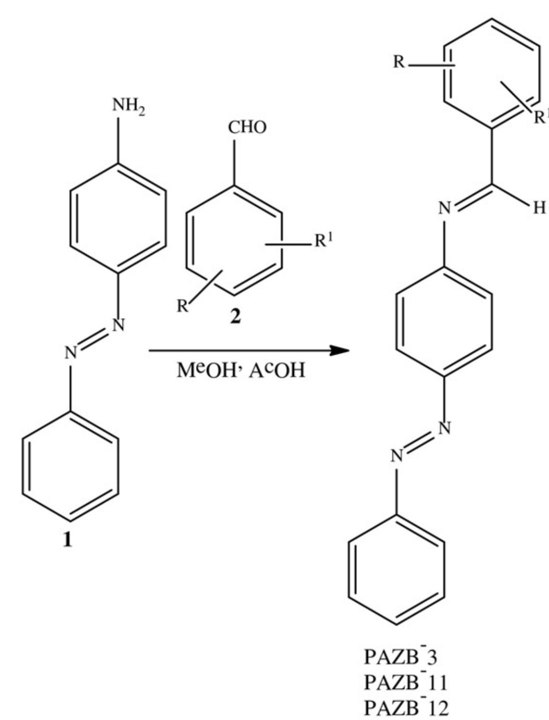

Fig. 1. Scheme of synthesis of the compounds PAZB-3, PAZB-11 and PAZB-12.

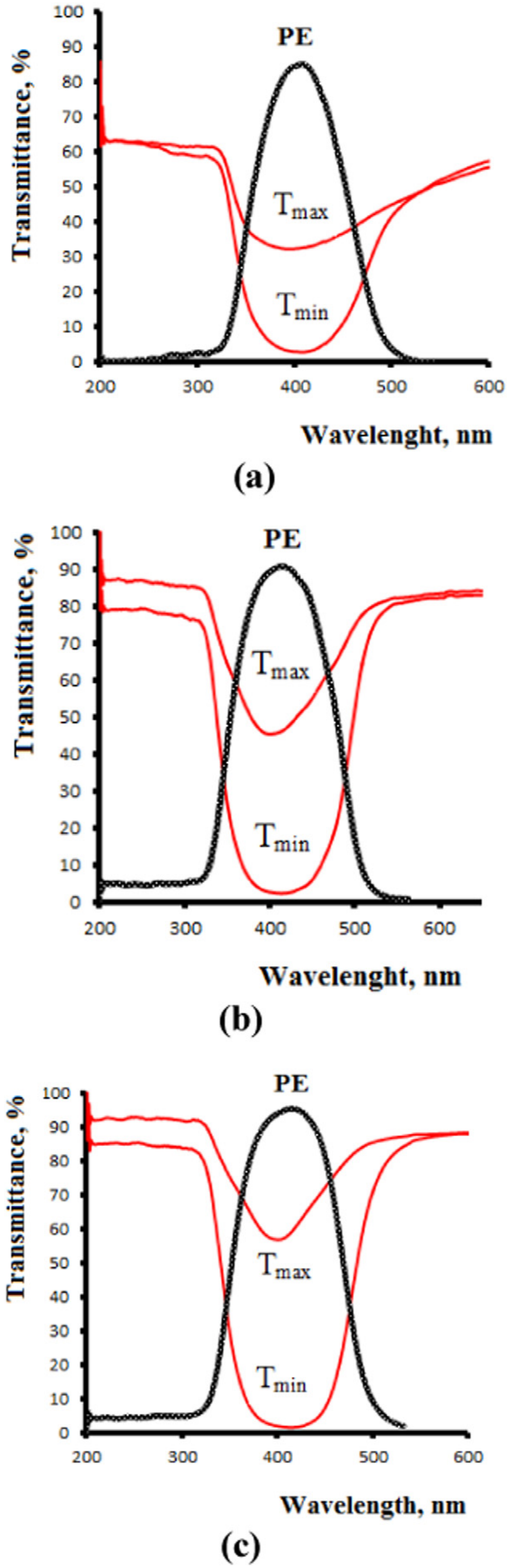

Fig. 2. Transmission spectra (T_{max}, T_{min}) and polarizing efficiency (PE) of polarizing PVA-films containing 0.30 wt% of the compounds PAZB-3 (a), PAZB-11 (b), PAZB-12 (c).

Table 1
Dependence of thermal conductivity on stretching degree in pure PVA-films.

R_s	λ		
	$\lambda_{\parallel}$, W/m·°C	$\lambda_{\perp}$, W/m·°C	$\lambda_{\parallel}/\lambda_{\perp}$
1.0	0.875	0.872	1.00
1.5	0.876	0.764	1.15
2.0	0.878	0.636	1.38
2.5	0.880	0.549	1.60
3.0	0.881	0.503	1.75
4.0	0.882	0.475	1.86

the UV/Vis spectra of the title dye in $CHCl_3$, DMSO and DMF solvents, the λ_{max} observed in the range of 345–355 nm that related to the $\pi \rightarrow \pi^*$ transitions of π electrons in the molecule. Also, the dye did not show any activity against gram negative bacteria. In another study, structural and optical properties of three symmetrical azomethines with long aliphatic chains were investigated [23]. In the UV/Vis absorption spectra of three azomethines in chloroform solution, the azomethines SAz1–SAz3 in the UV/Vis absorption spectra in chloroform solution exhibited two bands in the range of 323–346 nm and 282–294 nm. They detected the azomethine with one (SAz1) or two (SAz2) phenyl rings between imine (—C═N—) groups emitted violet or blue light respectively, while azomethine with methylene unit between the phenyl rings (SAz3) exhibited green light emission. In previous works, we reported the results of TD-DFT calculations for the oxazine dyes [13,14]. Also, we have investigated the molecular geometry optimizations and absorption bonds in UV/Vis spectrum of Azure A chloride by DFT and TD-DFT methods and it has concluded that experimental data are in excellent agreement with theoretical results [18]. In our current work, we designed three new azomethine dyes and modeled their geometrical parameters, UV/Vis and IR spectra by DFT methods. Frontier molecular orbitals, detail of quantum molecular descriptors, molecular electrostatic potential, natural charge and natural bond orbital analysis of the new compounds were calculated.

2. Experimental

2.1. Reagent and Apparatus

All chemical used were of analytical reagent grade. PVA "Mowiol 28–99" was manufactured by the Hoëchst Aktiengesllschaft Co., Germany. The UV/Vis spectrum of the compounds and PVA-films was recorded on UV–Visible Spectrophotometer Cary 300 (Varian, USA). The optical transmission spectra were measured in polarized light with a UV-NIR Spectrophotometer HR 4000 (Ocean optics, USA). Experimental FTIR spectra of the structures were recorded in the frequency region 400–4000 cm^{-1} on a Spectrophotometer of Protégé 460 (Nicolet, US). The thermal and electrical conductivity of PVA-films was measured on the complex equipment LC-201 (Alfa Laval Group, Sweden).

Table 2
Thermal conductivity of PVA-films containing the title compounds at concentration 0.3 wt%.

PVA + Dye	R_s	λ		
		$\lambda_{\parallel}$, W/m·°C	$\lambda_{\perp}$, W/m·°C	$\lambda_{\parallel}/\lambda_{\perp}$
PVA + PAZB-3	2.0	0.864	0.258	3.35
	3.0	0.850	0.236	3.60
	4.0	0.845	0.189	4.47
	5.0	0.832	0.087	9.56
PVA + PAZB-11	2.0	0.874	0.257	3.40
	3.0	0.870	0.201	4.32
	4.0	0.848	0.191	4.44
	5.0	0.834	0.080	10.43
PVA + PAZB-12	2.0	0.862	0.246	3.50
	3.0	0.871	0.189	4.61
	4.0	0.842	0.150	5.61
	5.0	0.833	0.083	10.04

Table 3
Dependence of electrical conductivity on stretching degree in pure PVA-films.

R_s	δ		
	$\delta_{\parallel}$, S·cm^{-1}	$\delta_{\perp}$, S·cm^{-1}	$\delta_{\parallel}/\delta_{\perp}$
1.0	$1.1 \cdot 10^5$	$1.1 \cdot 10^5$	$1.0 \cdot 10^0$
1.5	$4.6 \cdot 10^5$	$8.4 \cdot 10^4$	$0.5 \cdot 10^1$
2.0	$9.8 \cdot 10^5$	$1.7 \cdot 10^4$	$5.7 \cdot 10^1$
2.5	$3.6 \cdot 10^6$	$2.2 \cdot 10^3$	$1.6 \cdot 10^3$
3.0	$7.8 \cdot 10^7$	$5.7 \cdot 10^2$	$1.3 \cdot 10^5$

2.2. Preparation of Polarizing PVA-films Containing the Title Compounds

The PVA-films were prepared from (wt%) 10 PVA solution containing 0.01–0.03 **PAZB-3**, **PAZB-11**, **PAZB-12** (0.10–0.30 in film), 0.01 boric acid (H_3BO_3), 6.0 ethyl alcohol (C_2H_5OH) and water. An initial composition was prepared by dissolving PVA (powder) in distilled water and ethyl alcohol. The composition was mixed at temperature 85–90 °C. The title compounds and additives were added after 3 h after starting of heating PVA solution at intervals 20 min. The mixture was heated for 3 h. The hot solution was filtered through two layers of technical nylon (NMO600 filter, Yueqing SaiLao Qi Gauze filter Co.). De-aeration occurred during12–15 h. The composition was cast on the polished glass surface and dried in a closed box at temperature 20–22 °C. Uniaxial orientation was done in the 4% boric acid solution at temperature 42–45 °C. The washed film was dried for 30 min at temperature 60–63 °C. The value of Stretching Degree (R_s) was determined as the ratio between length of the films after and before (l_{aft}/l_{bef}) uniaxial orientation. The thickness of the resulting films was between 50 and 55 μm. The film thickness was measured with a micrometer with an accuracy of ± 5 μm (GS SSSR6507-90).

Accuracy of measurements in this research limits the accuracy of the results:

- Sample of the starting composition for preparation of solutions and films for casting taken on an analytical balance accurate to 0.0005 g;
- Temperature measurement error was:
  ± 2.0 °C in the preparation of polymer solutions with additives,
  ± 1.0 °C in the chemical treatment of the films,
  ± 3.0 °C at thermal fixation and drying films;
- Relative error of spectrophotometric analysis did not exceed 1.0% and thermal conductivity 0.1%.

The standard deviation of parallel measurements determined by the formula [10]:

$$S(d) = \sqrt{\sum_i (d_i - d)^2 / n - 1} \tag{1}$$

Table 4
Electrical conductivity of PVA-films containing the title compounds at concentration 0.3 wt%.

PVA + Dye	R_s	δ		
		$\delta_{\parallel}$, S.cm^{-1}	$\delta_{\perp}$, S.cm^{-1}	$\delta_{\parallel}/\delta_{\perp}$
PVA + PAZB-3	2.0	$3.1 \cdot 10^5$	$5.3 \cdot 10^4$	$5.8 \cdot 10^0$
	3.0	$6.2 \cdot 10^7$	$6.8 \cdot 10^2$	$0.9 \cdot 10^5$
	4.0	$8.7 \cdot 10^7$	$5.4 \cdot 10^1$	$1.6 \cdot 10^6$
	5.0	$4.9 \cdot 10^8$	$1.1 \cdot 10^1$	$4.5 \cdot 10^7$
PVA + PAZB-11	2.0	$6.4 \cdot 10^5$	$3.1 \cdot 10^4$	$2.1 \cdot 10^1$
	3.0	$7.7 \cdot 10^7$	$3.5 \cdot 10^2$	$2.2 \cdot 10^5$
	4.0	$5.8 \cdot 10^8$	$4.7 \cdot 10^1$	$1.2 \cdot 10^7$
	5.0	$3.3 \cdot 10^9$	$5.0 \cdot 10^0$	$0.6 \cdot 10^9$
PVA + PAZB-12	2.0	$5.2 \cdot 10^5$	$3.7 \cdot 10^4$	$1.4 \cdot 10^1$
	3.0	$7.8 \cdot 10^7$	$3.4 \cdot 10^2$	$2.3 \cdot 10^5$
	4.0	$6.3 \cdot 10^8$	$5.1 \cdot 10^2$	$1.2 \cdot 10^6$
	5.0	$4.5 \cdot 10^9$	$2.9 \cdot 10^2$	$1.6 \cdot 10^7$

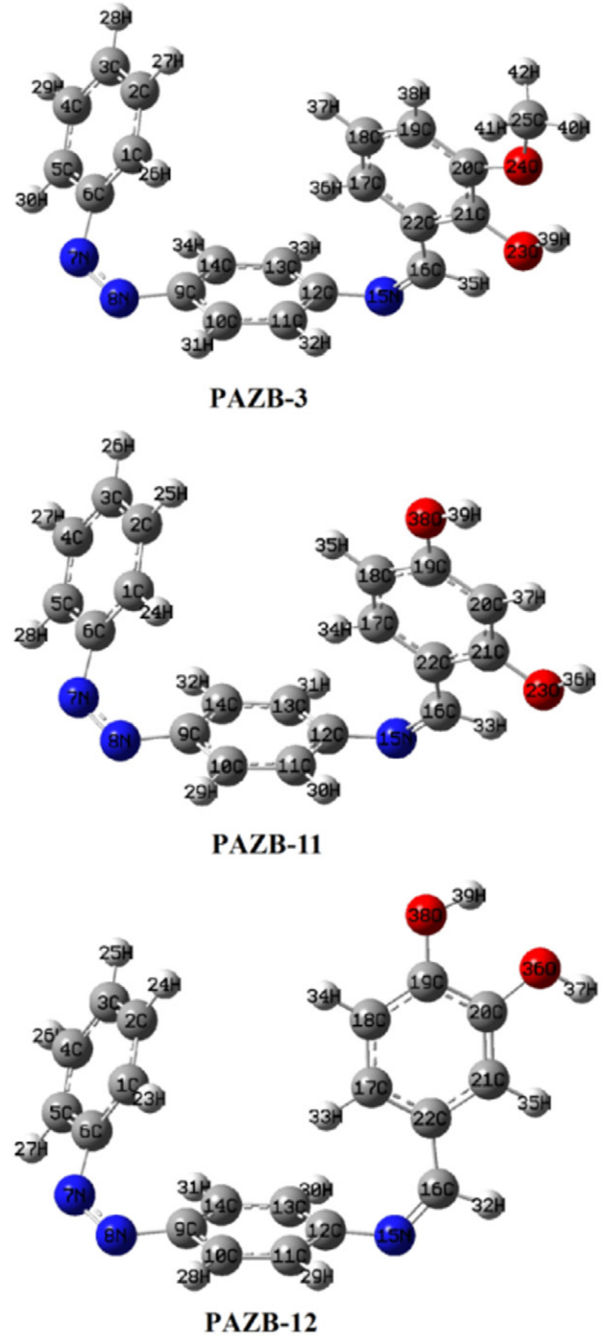

Fig 3. Optimized molecular structures of the compounds PAZB-3, PAZB-11, PAZB-12 calculated by PBE1PBE/6-31 + G method.

where d_i—the result of a single measurement,d—arithmetic mean,n—number of measurements.

2.3. Synthesis of the Compounds PAZA-3, PAZB-11, PAZB-12

2.3.1. PAZB-3

A mixture of 4-aminoazobenzne (1) (2.6 mmol) and aldehyde (2) (2.3 mmol) in 42 ml methanol was prepared. 2 ml of glacial acetic acid was added to the mixture and was refluxed for 1 h. The hot solution was filtered through a paper filter, cooled and left for 15 h. at 2–7 °C. The solid was dissolved in cold methanol and washed with water and dried at 23–25 °C.

Table 5
Selected optimized geometrical parameters (Bond lengths (Å) and Bond angles (°)) of the compound PAZB-3 calculated by PBE1PBE/6-31+G method.

Parameter	Bond lengths (Å)		Parameter	Bond angles (°)	
	Experimental	Calculated		Experimental	Calculated
C1-C2	1.391	1.394	C1-C2-C3	120.48	120.40
C1-C6	1.395	1.403	C1-C6-C5	120.33	120.29
C2-C3	1.399	1.400	C1-C6-N7	122.10	122.06
C3-C4	1.390	1.398	C2-C3-C4	119.92	119.83
C4-C5	1.399	1.395	C4-C5-C6	119.80	119.78
C5-C6	1.403	1.399	C5-C6-N7	117.04	117.03
C6-N7	1.431	1.438	C6-N7-N8	124.44	124.40
N7-N8	1.273	1.265	N7-N8-C9	124.80	124.79
N8-C9	1.438	1.430	C9-C10-C11	120.53	120.54
C9-C10	1.400	1.402	C10-C11-C12	120.04	120.02
C9-C14	1.409	1.405	C10-C9-C14	119.50	119.49
C10-C11	1.396	1.389	C12-C13-C14	120.53	120.55
C11-C12	1.402	1.407	C13-C12-N15	119.40	119.36
C12-C13	1.403	1.407	C11-C12-N15	120.95	120.99
C12-N15	1.403	1.403	C12-N15-C16	126.94	126.98
C13-C14	1.394	1.389	N15-C16-C22	130.15	130.14
N15-C16	1.294	1.289	C16-C22-C17	124.35	124.39
C16-C22	1.473	1.467	C17-C18-C19	120.77	120.74
C17-C18	1.394	1.389	C17-C22-C21	117.95	117.99
C17-C22	1.415	1.412	C18-C19-C20	119.01	119.00
C18-C19	1.410	1.404	N15-C16-H35	115.32	115.30
C19-C20	1.383	1.388	C21-O23-H39	109.75	109.79
C20-C21	1.410	1.404	C20-C24-C25	118.96	118.99
C20-O24	1.384	1.383	C21-C20-O24	113.06	113.09
C21-C22	1.403	1.401	C22-C21-O23	120.18	120.15
C21-O23	1.380	1.377	C19-C20-O24	126.45	126.42
O24-C25	1.455	1.452	C16-C22-C21	117.47	117.49

2.3.2. PAZB-11

A mixture of 4-aminoazobenzne (1) (2.3 mmol) and aldehyde (2) (2.5 mmol) in 37 ml methanol was prepared. 3 ml of glacial acetic acid was added to the mixture and was refluxed for 2 h. The hot solution was filtered through a paper filter, cooled and left for 10 h. at 1–4 °C. The solid was dissolved in cold methanol and washed with water and dried at 22–25 °C.

Table 6
Selected optimized geometrical parameters (Bond lengths (Å) and Bond angles (°)) of the compound PAZB-11 calculated by PBE1PBE/6-31+G method.

Parameter	Bond lengths (Å)		Parameter	Bond angles (°)	
	Experimental	Calculated		Experimental	Calculated
C1-C2	1.397	1.394	C1-C2-C3	120.43	120.39
C1-C6	1.407	1.403	C1-C6-C5	120.27	120.29
C2-C3	1.405	1.400	C1-C6-N7	121.93	121.89
C3-C4	1.401	1.398	C2-C3-C4	119.94	119.82
C4-C5	1.402	1.396	C4-C5-C6	119.84	119.76
C5-C6	1.401	1.399	C5-C6-N7	117.33	117.21
C6-N7	1.437	1.438	C6-N7-N8	124.40	124.31
N7-N8	1.262	1.266	N7-N8-C9	124.77	124.79
N8-C9	1.436	1.430	C9-C10-C11	120.59	120.57
C9-C10	1.408	1.402	C10-C11-C12	120.10	120.07
C9-C14	1.410	1.405	C10-C9-C14	119.55	119.43
C10-C11	1.384	1.389	C12-C13-C14	120.69	120.61
C11-C12	1.400	1.408	C13-C12-N15	119.50	119.47
C12-C13	1.401	1.408	C11-C12-N15	121.00	120.98
C12-N15	1.400	1.401	C12-N15-C16	127.42	127.31
C13-C14	1.402	1.389	N15-C16-C22	130.51	130.46
N15-C16	1.296	1.291	C16-C22-C17	124.47	124.41
C16-C22	1.460	1.462	C17-C18-C19	119.20	119.17
C17-C18	1.392	1.386	C17-C22-C21	117.31	117.25
C17-C22	1.402	1.409	C18-C19-C20	120.90	120.86
C18-C19	1.401	1.399	N15-C16-H33	115.11	115.07
C19-C20	1.402	1.395	C21-O23-H36	113.40	113.37
C19-O38	1.377	1.377	C20-C19-O38	122.38	122.30
C20-C21	1.398	1.394	C18-C19-O38	116.90	116.83
C21-C22	1.406	1.412	C20-C21-O23	121.31	121.22
C21-O23	1.381	1.379	C22-C21-O23	117.11	117.06

Table 7
Selected optimized geometrical parameters (Bond lengths (Å) and Bond angles (°)) of the compound PAZB-12 calculated by PBE1PBE/6-31+G method.

Parameter	Bond lengths (Å)		Parameter	Bond angles (°)	
	Experimental	Calculated		Experimental	Calculated
C1-C2	1.391	1.394	C1-C2-C3	120.45	120.39
C1-C6	1.409	1.403	C1-C6-C5	12,033	120.30
C2-C3	1.408	1.400	C1-C6-N7	121.89	121.91
C3-C4	1.400	1.398	C2-C3-C4	119.71	119.82
C4-C5	1.399	1.396	C4-C5-C6	119.85	119.75
C5-C6	1.394	1.399	C5-C6-N7	117.20	117.17
C6-N7	1.430	1.438	C6-N7-N8	124.38	124.41
N7-N8	1.270	1.266	N7-N8-C9	125.11	125.03
N8-C9	1.436	1.430	C9-C10-C11	120.64	120.67
C9-C10	1.409	1.402	C10-C11-C12	120.07	120.02
C9-C14	1.411	1.405	C10-C9-C14	119.40	119.38
C10-C11	1.400	1.389	C12-C13-C14	120.56	120.53
C11-C12	1.401	1.406	C13-C12-N15	120.51	120.47
C12-C13	1.415	1.409	C11-C12-N15	119.91	119.89
C12-N15	1.397	1.400	C12-N15-C16	128.13	128.11
C13-C14	1.395	1.389	N15-C16-C22	131.51	131.35
N15-C16	1.296	1.288	C16-C22-C17	124.90	124.94
C16-C22	1.468	1.467	C17-C18-C19	119.89	119.94
C17-C18	1.390	1.393	C17-C22-C21	118.88	118.92
C17-C22	1.412	1.407	C18-C19-C20	120.00	120.02
C18-C19	1.399	1.391	N15-C16-H32	114.77	114.71
C19-C20	1.415	1.402	C20-O36-H37	114.65	114.60
C19-O38	1.377	1.374	C20-C19-O38	119.92	119.94
C20-C21	1.383	1.384	C18-C19-O38	120.06	120.02
C20-O36	1.390	1.385	C21-C20-O36	125.70	125.71
C21-C22	1.406	1.411	C19-C20-O36	113.91	113.93

2.3.3. PAZB-12

A mixture of 4-aminoazobenzne (1) (3.1 mmol) and aldehyde (2) (2.4 mmol) in 26 ml methanol was prepared. 3 ml of glacial acetic acid was added to the mixture and was refluxed for 4 h. The hot solution was filtered through a paper filter, cooled and left for 7 h. at 10 °C. The solid was dissolved in cold methanol and washed with water and dried at 22–25 °C (Fig. 1).

2.4. Optical Anisotropy of PVA-films Containing the Compounds PAZB-3, PAZB-11, PAZB-12

The main optical properties of polarizing PVA-films such as Transmittance (T_{max}, T_{min}) and Polarizing Efficiency (PE) were evaluated at

Table 8
Comparison of the calculated λ_{max} by PBE1PBE, PBE1PBE, B3LYP methods with 6-31G, 6-31+G, 6-31+G*, 6-31++G* basis sets.

Method	Basis set	PAZB-3 ($\lambda_{max, exp.}$ = 371 nm)		PAZB-11 ($\lambda_{max, exp.}$ = 375 nm)		PAZB-12 ($\lambda_{max, exp.}$ = 377 nm)	
		$\lambda_{max, cal.}$	f	$\lambda_{max, cal.}$	f	$\lambda_{max, cal.}$	f
PBE1PBE	6-31G	251	0.31	368	0.21	344	0.33
	6-31+G	256	0.28	372	0.23	282	0.23
	6-31+G*	255	0.19	359	0.24	284	0.22
	6-31++G*	255	0.19	359	0.24	284	0.22
PBEPBE	6-31G	445	0.25	445	0.21	436	0.25
	6-31+G	295	0.21	451	0.17	441	0.21
	6-31+G*	575	0.16	571	0.17	424	0.16
	6-31++G*	574	0.15	570	0.17	423	0.16
B3LYP	6-31G	431	0.86	437	1.45	433	1.45
	6-31+G	432	1.15	441	1.48	425	1.35
	6-31+G*	425	1.35	438	1.48	435	1.47
	6-31++G*	425	1.35	438	1.48	435	1.47

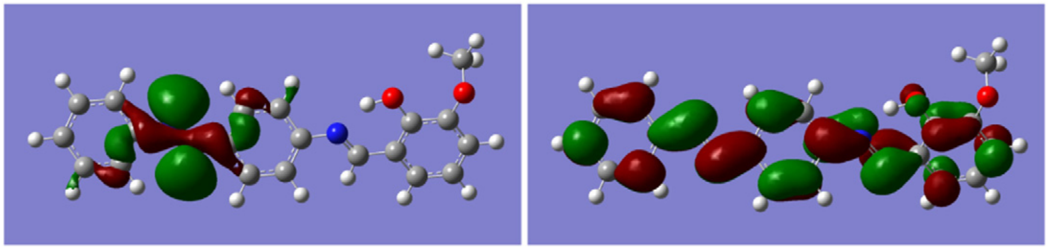

Fig. 4. Form of the MO involved in formation of absorption spectrum of the compound PAZB-3 at $\lambda_{max} = 425$ nm calculated by B3LYP/6-31++G* method.

the absorption maximum of the polarizing films according to Eq. (2) [13]:

$$PE = (T_{max} - T_{min})/(T_{max} + T_{min}) * 100 \quad (2)$$

where, T_{max}, T_{min}—transmittance for linearly polarized light parallel and perpendicular to direction of stretching of colored PVA-film. Multi-angle spectral photometric measurements were performed for all samples in the spectral range from 200 to 600 nm at incidence angles of 7°, 10°, 20°, 30°, and 40° for s- and p-polarized light. In all optical characterization and reverse-engineering procedures throughout this study, we used measurement data taken in the spectral range from 300 to 500 nm only. Polarizing Efficiency (PE) of colored oriented PVA-films depends on the concentration of synthesized dyes (PAZB-3, PAZB-11 and PAZB-12) and Stretching Degree ($R_s = 3.5$) of the films, therefore the optimum concentration of the PAZB-3, PAZB-11 and PAZB-12 in PVA-film was obtained (Fig. 2a, b, c).

Change in concentration of the title compounds from 0.10 to 0.30 wt% in the colored oriented PVA-film show that with increasing concentration maximum light transmission in parallel and perpendicular direction are reduced. At [PAZB-3] = 0.30 wt% $T_{max} = 33.3\%$, $T_{min} = 0.25\%$. PVA-film effectively polarizes the light at 409 nm of spectrum with PE = 90%. At [PAZB-11] = 0.30 wt% $T_{max} = 47.5\%$, $T_{min} = 0.35\%$. PVA-film effectively polarizes the light at 411 nm of spectrum with PE = 95%. At [PAZB-12] = 0.30 wt% $T_{max} = 58.5\%$, $T_{min} = 0.15\%$. PVA-film effectively polarizes the light at 410 nm of spectrum with PE = 96%.

2.5. Anisotropy of Thermal Conductivity of PVA-films Containing the PAZB-3, PAZB-11, PAZB-12

In the present study, we have studied anisotropy of thermal conductivity of the dyes in oriented colored PVA-films. The thermo-physical properties of films were determined by thermal conductivity of samples in parallel ($\lambda_{\|}$) and perpendicular ($\lambda_{\perp}$) directions of stretching axis. During this work, it was established that the oriented PVA-film has the phenomenon of *anisotropy of thermal conductivity* ($\lambda_{\|}/\lambda_{\perp}$). Thermal conductivity in a direction of orientation ($\lambda_{\|}$) is higher than in a direction perpendicular orientations ($\lambda_{\perp}$). Due to this anisotropy at a known degree of extension it is possible to judge anisotropy of chain structure. It has been noticed that during thermal expansion and thermal conductivity geometric parameters of molecule, intermolecular forces play a significant role. In unstretched PVA-film anisotropy of thermal conductivity is not observed appreciably ($\lambda_{\|} = 0.875$ W/m·°C; $\lambda_{\perp} = 0.869$ W/m·°C) whereas in stretched PVA-film anisotropy of thermal conductivity is observed clearly (Table 1).

When we add the dye to PVA-film there is change in its thermal conductivity (Table 2). It has been found that along an axis of orientation, it has increased, and in perpendicular axis it is decreased. Results of

Table 9
Electronic absorption spectrum of the compound PAZB-3 calculated by TDB3LYP/6-31++G*.

Excited state	Wavelength (nm)	Excitation energy (eV)	Configurations composition (corresponding transition orbitals)	Oscillator strength (f)
S_1	483	2.56	0.68(H-2 → L) − 0.17(H-2 → L + 1)	0.00
S_2	425	2.91	0.70(H → L)	1.35
S_3	383	3.23	0.70(H-1 → L)	0.28
S_4	329	3.76	−0.38(H-3 → L) + 0.56(H → L + 1)	0.01
S_5	322	3.84	0.65(H-4 → L) − 0.14(H-3 → L) − 0.13(H → L + 1)	0.02
S_6	316	3.91	0.66(H-5 → L) − 0.16(H → L + 2)	0.01
S_7	312	3.96	0.18(H-4 → L) + 0.53(H-3 → L) − 0.19(H-1 → L + 1) + 0.33(H → L + 1)	0.00
S_8	303	4.07	0.17(H-6 → L) + 0.17(H-3 → L) + 0.61(H-1 → L + 1)	0.02
S_9	297	4.16	0.15(H-8 → L) + 0.59(H-6 → L) − 0.19(H-2 → L + 1) − 0.21(H-1 → L + 1) − 0.10(H → L + 1)	0.03
S_{10}	296	4.17	0.18(H-6 → L) + 0.16(H-2 → L) + 0.64(H-2 → L + 1)	0.00
S_{11}	267	4.63	0.65(H-7 → L) + 0.13(H-7 → L + 1) + 0.11(H-6 → L + 1) − 0.15(H-3 → L + 1)	0.00
S_{12}	261	4.73	0.47(H-8 → L) + 0.15(H-8 → L + 1) − 0.22(H-6 → L) + 0.22(H-6 → L + 1) + 0.13(H-5 → L + 1) − 0.29(H-3 → L + 1)	0.09
S_{13}	256	4.82	−0.31(H-8 → L) + 0.37(H-5 → L+) − 0.37(H-3 → L + 1) − 0.27(H → L + 2)	0.11
S_{14}	254	4.86	0.15(H-8 → L) + 0.42(H-5 → L + 1) + 0.41(H-3 → L + 1) − 0.25(H → L + 2) − 0.10(H → L + 4)	0.02
S_{15}	250	4.95	0.24(H-5 → L + 1) − 0.11(H-4 → L) − 0.41(H-4 → L + 1) + 0.42(H → L + 2) + 0.17(H → L + 3)	0.05
S_{16}	248	4.99	0.11(H-5 → L) + 0.30(H-5 → L + 1) + 0.39(H-4 → L + 1) + 0.35(H → L + 2) − 0.28(H → L + 3)	0.03
S_{17}	246	5.03	−0.25(H-8 → L) + 0.14(H-8 → L + 1) + 0.53(H-6 → L + 1) + 0.17(H-3 → L + 1) + 0.22(H-2 → L + 2)	0.00
S_{18}	245	5.04	−0.18(H-6 → L + 1) + 0.66(H-2 → L + 2)	0.00
S_{19}	238	5.19	−0.12(H-4 → L + 1) + 0.66(H-2 → L + 3) − 0.18(H → L + 3)	0.00
S_{20}	238	5.19	0.10(H-6 → L + 1) + 0.35(H-4 → L + 1) + 0.23(H-2 → L + 3) + 0.52(H → L + 3)	0.04

H-HOMO, L-LUMO.

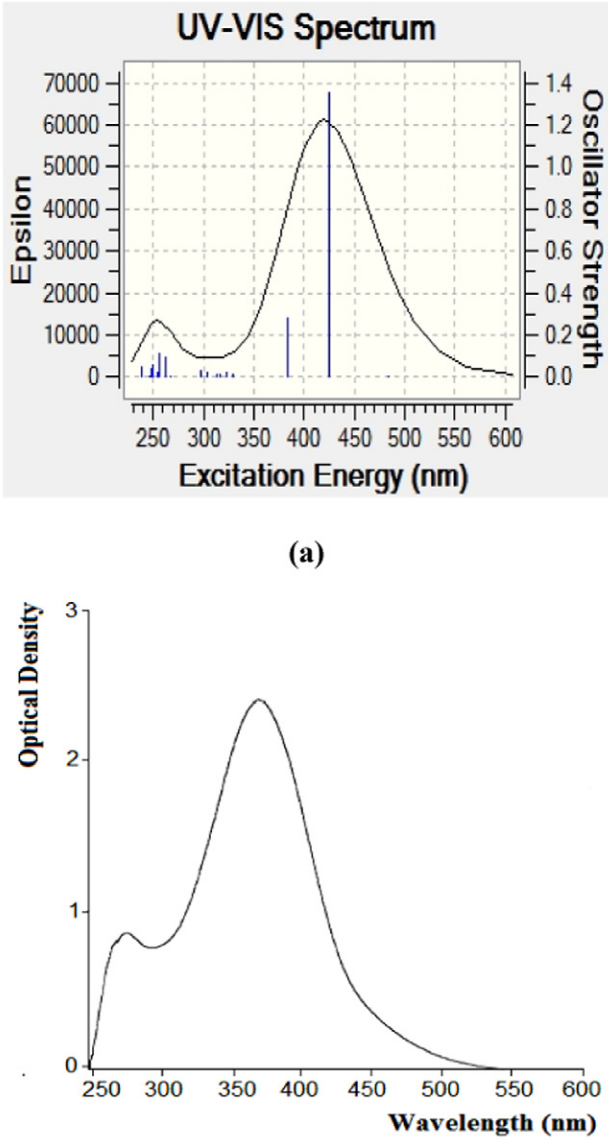

(a)

(b)

Fig. 5. UV/Vis spectrum of the compound PAZB-3 in solvent DMF: a) calculated by TDPB3LYP/6-31++G* method and b) experimental at concentration of dye $4.2 \cdot 10^{-4}$ M.

thermal conductivity measurements of PVA-films containing the title compounds are presented in the Table 2.

The occurrence of anisotropy of thermal conductivity is connected that at orientation of PVA-film occurs orientation of the amorphous part of polymer and formation of additional number of intermolecular connections. Thermal conductivity of PVA-films changes after adding of the dyes (Table 2) and along an axis of orientation and in perpendicular axis decreases.

2.6. Anisotropy of Electrical Conductivity of PVA-films Containing the PAZB-3, PAZB-11, PAZB-12

In the present section, we have studied electrical conductivity of the PVA-films with PAZB-3, PAZB-11 and PAZB-12. Electrical conductivity of PVA-films was measured on the complex equipment LC-201(Alfa Laval Group, Sweden). The PVA-films were placed on the surface of the thin sheet (electrode) from SnO_2 (thickness 70 μm). And then the films were coated with an aluminum electrode ($S = 2.5$ cm^2). The thickness of the PVA samples was 55 μm. The electrical conductivity of PVA-films was measured in parallel ($\delta_{\|}$) and perpendicular ($\delta_{\perp}$) directions of stretching axis. In unstretched PVA-film anisotropy of electrical conductivity is not observed ($\delta_{\|} = 1.1 \cdot 10^5$ S·cm^{-1}; $\delta_{\perp} = 1.1 \cdot 10^5$ S·cm^{-1}) whereas in stretched PVA-film anisotropy of electrical conductivity is observed very clearly (Table 3).

After adding the dyes to PVA-films there is change in its electrical conductivity (Table 4). It has been found that along an axis of orientation, it has increased, and in perpendicular axis it is reduced. Anisotropy of electrical conductivity of PVA-films was defined as $\delta_{\|}/\delta_{\perp}$ and is presented in Table 4.

3. Computational Methods

The quantum chemical calculations were performed using the Gaussian 09W software program [24] on a Pentium IV/4.28 GHz personal computer. The geometry of the title structures: PAZB-3, PAZB-11, PAZB-12 was fully optimized using GaussView 05 program by gradient geometry optimization. The frequencies (theoretical IR spectra) and structural parameters of the three new azomethine compounds were calculated using functional PBE1PBE (One-parameter hybrid PBE functional incorporating 25% HF exchange) with 6-31+G basis set for the optimized geometries in a solvent DMF. Without any constraint on the geometry the energies of the title molecules were minimized, whole intramolecular forces were brought to be zero. We also used TD-DFT for computing the electronic transitions of new azomethine structures. The Polarized Continuum Model (PCM) [21] was used for calculations of solvent effect. Theoretical absorption spectrum of the title structures in a solvent DMF was calculated using TDPBE1PBE, TDPBEPBE, TDB3LYP methods with 6-31G, 6-31+G, 6-31+G*, 6-31++G* method. The electronic properties such as dipole moment (μ_D), point group, E_{HOMO}, E_{LUMO}, HOMO-LUMO energy gap and natural charges were calculated [25]. The optimized molecular structure, HOMO and LUMO surfaces were visualized using GaussView 05 program [26]. The electronic structure of the compound PAZB-11 were studied by using Natural Bond Orbital (NBO) analysis [25] using PBE1PBE/6-31+G level of energy in order to understand hyper conjugative interactions and charge delocalization.

3.1. Optimized Structure of the Compounds PAZB-3, PAZB-11, PAZB-12

We have carried out quantum chemical calculations and have optimized structure of the three compounds: PAZB-3, PAZB-11, PAZB-12 using PBE1PBE, PBE1PBE, B3LYP methods with 6-31G, 6-31+G, 6-31+G*, 6-31++G* basis set by Gaussian 09W program package. The calculations were performed in solvent DMF using the IEFPCM (Integral Equation Formalism PCM) method coupled to UAKS radii. The optimized molecular structures by PBE1PBE/6-31+G level of energy and parameters of the studied structures are shown in Fig. 3 and Tables 5, 6, 7. The Integral Equation Formalism PCM, by Cances, Mennucci and Tomasi is the most popular PCM version.

3.2. Electronic Structure and Excited States of the Compounds PAZB-3, PAZB-11, PAZB-12

We used the Time-dependent density functional theory (TD-DFT) for predicting the absorption spectra of the compounds PAZB-3, PAZB-11, PAZB-12. The theoretical absorption spectra of the optimized compounds were calculated in solvent DMF using the TDPBE1PBE, TDPBEPBE, TDB3LYP methods with 6-31G, 6-31+G, 6-31+G*, 6-31++G* basis sets. The calculated maximum wavelength (λ_{max}) of the title compounds is reported in Table 8.

The better absorption spectrum for the compounds PAZB-3, PAZB-11, PAZB-12 obtained using TDB3LYP/6-31++G*, TDPBE1PBE/6-

Table 10
Electronic absorption spectrum of the compound PAZB-11 calculated by TDPBE1PBE/6-31+G.

Excited state	Wavelength (nm)	Excitation energy (eV)	Configurations composition (corresponding transition orbitals)	Oscillator strength (f)
S_1	511	2.42	−0.10(H-5 → L) + 0.23(H-2 → L) + 0.18(H-1 → L) + 0.61(H → L)	0.09
S_2	372	3.33	0.33(H-2 → L) − 0.10(H-2 → L + 1) + 0.32(H-1 → L) − 0.27(H → L) + 0.40(H → L + 1)	0.23
S_3	346	3.57	−0.19(H-2 → L) − 0.20(H-2 → L + 1) − 0.34(H-1 → L) + 0.15(H → L) + 0.50(H → L + 1)	0.08
S_4	322	3.84	0.50(H-2 → L) − 0.47(H-1 → L)	0.03
S_5	304	4.06	−0.28(H-5 → L) + 0.50(H-4 → L) − 0.30(H-3 → L) − 0.12(H-2 → L) + 0.13(H → L + 2)	0.03
S_6	294	4.20	−0.21(H-6 → L) + 0.53(H-5 → L) + 0.23(H-4 → L) − 0.13(H-3 → L) + 0.23(H → L + 2)	0.06
S_7	286	4.33	0.28(H-6 → L) + 0.21(H-5 → L) + 0.29(H-4 → L) + 0.31(H-3 → L) − 0.12(H-3 → L + 1) + 0.21(H-2 → L + 1) − 0.21(H-1 → L + 1) − 0.16(H → L + 2) + 0.13(H → L + 3)	0.02
S_8	281	4.39	0.35(H-6 → L) + 0.13(H-5 → L) − 0.11(H-3 → L) + 0.12(H-3 → L + 1) − 0.17(H-2 → L + 1) + 0.41(H-1 → L + 1) − 0.27(H → L + 2) + 0.11(H → L + 5)	0.18
S_9	277	4.46	−0.11(H-4 → L) + 0.53(H-2 → L + 1) + 0.31(H-1 → L + 1) + 0.22(H → L + 1) + 0.11(H → L + 2)	0.01
S_{10}	273	4.52	−0.13(H-5 → L) + 0.15(H-4 → L) + 0.50(H-3 → L) − 0.16(H-2 → L + 1) + 0.29(H-1 → L + 1) + 0.25(H → L + 2)	0.13
S_{11}	268	4.62	0.39(H-6 → L) − 0.19(H-4 → L) − 0.12(H-1 → L + 1) + 0.46(H → L + 2) + 0.15(H → L + 3)	0.14
S_{12}	254	4.87	0.47(H-3 → L + 1) − 0.17(H-1 → L + 1) − 0.20(H-1 → L + 2) − 0.10(H-1 → L + 4) − 0.32(H → L + 3) + 0.16(H → L + 4)	0.09
S_{13}	252	4.91	−0.23(H-6 → L) + 0.25(H-3 → L + 1) − 0.11(H-1 → L + 3) + 0.50(H → L + 3) + 0.17(H → L + 4) + 0.12(H → L + 5)	0.06
S_{14}	246	5.03	−0.23(H-3 → L + 1) − 0.10(H-2 → L + 2) + 0.59(H → L + 4)	0.06
S_{15}	239	5.16	−0.23(H-6 → L + 1) − 0.12(H-5 → L + 1) + 0.41(H-4 → L + 1) − 0.11(H-3 → L + 1) + 0.11(H-2 → L + 2) − 0.14(H → L + 3) + 0.36(H → L + 5) + 0.10(H → L + 7)	0.01
S_{16}	238	5.20	−0.11(H-7 → L) + 0.14(H-6 → L + 1) + 0.13(H-5 → L + 1) − 0.30(H-4 → L + 1) − 0.21(H-2 → L + 2) − 0.15(H-1 → L + 2) + 0.48(H → L + 5)	0.00
S_{17}	236	5.25	−0.14(H-4 → L + 1) + 0.13(H-3 → L + 1) + 0.26(H-2 → L + 2) + 0.53(H-1 → L + 2) − 0.14(H → L + 3) + 0.11(H → L + 4) + 0.13(H → L + 5)	0.01
S_{18}	235	5.26	0.13(H-9 → L) + 0.62(H-7 → L)	0.04
S_{19}	230	5.38	−0.11(H-2 → L + 2) − 0.42(H → L + 6) + 0.13(H → L + 7) − 0.53(H → L + 8)	0.03
S_{20}	228	5.42	−0.17(H-4 → L + 1) − 0.13(H-3 → L + 1) + 0.47(H-2 → L + 2) − 0.31(H-1 → L + 2) + 0.24(H → L + 7)	0.08

H-HOMO, L-LUMO.

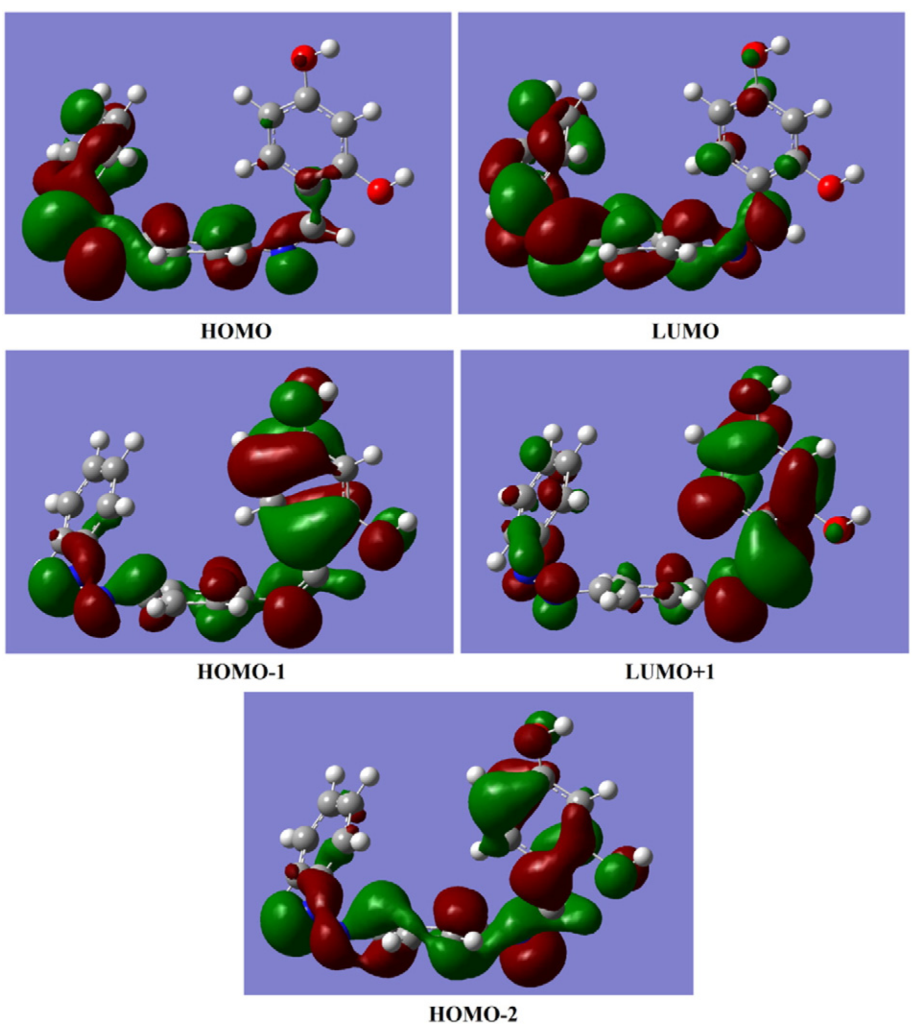

Fig. 6. Form of the MO involved in formation of absorption spectrum of the compound PAZB-11 at λ_{max} = 372 nm calculated by PBE1PBE/6-31+G method.

31 + G and TDPBE1PBE/6-31G, respectively. We considered 20 excited states and the computational equations were performed using the IEFPCM (Integral Equation Formalism PCM) method coupled to UAKS radii. The accurate value of absorption wavelength is obtained using the TD-DFT method.

According to theoretical calculations, the strong peak at $\lambda_{max} =$ 425 nm and the oscillator strength f = 1.35 in electronic absorption spectrum of the compound PAZB-3 is due to Charge-Transfer (CT) of one electron into the excited singlet state $S_0 \rightarrow S_2$, which it describes by a wave function corresponding to configuration for one-electron excitation [(HOMO) → (LUMO)] (Fig. 4). Also, excitation of one electron at 383 nm (f = 0.28) belonged to the transition into the state $S_0 \rightarrow S_3$ and describes by a wave function corresponding to a superposition of one configuration for one-electron excitation [(H-1 → L)]. The other excited states of the title compound have very small intensity (f ≈ 0) that is nearly forbidden by orbital symmetry considerations (Table 9).

The calculated UV/Vis spectrum of the compound PAZB-3 in solvent DMF and experimental spectrum at concentration 1 M/L and in solvent DMF is observed in Fig. 5a, b. The calculated and experimental magnitudes of maximum wavelength (λ_{max}) are 425 nm (f = 1.35, Fig. 5a) and 371 nm (D = 2.386, Fig. 5b), respectively.

In electronic absorption spectrum of the compound PAZB-11, the maximum wavelength with the highest oscillation are observed at 372 nm and f = 0.23 (Table 10). Calculations show transitions [(H-2 → L), (H-2 → L + 1), (H-1 → L), (H → L), (H → L + 1)] are the most important Charge-Transfer in the compound PAZB-11 with absorption peak at 372 nm (Fig. 6) that belong to the transition of one electron into the excited singlet state $S_0 \rightarrow S_2$. Excitation of one electron at 281 nm (f = 0.18) belonged to the transition into the state $S_0 \rightarrow S_8$ and describes by a wave function corresponding to a superposition of eight configurations for one-electron excitations [(H-6 → L), (H-5 → L), (H-3 → L), (H-3 → L + 1), (H-2 → L + 1), (H-1 → L + 1), (H → L + 2), (H → L + 5)]. The other excited states of the title compound have very small intensity (f ≈ 0) and are nearly forbidden by orbital symmetry considerations (Table 10).

The calculated UV/Vis spectrum of the compound PAZB-11 in solvent DMF and experimental spectrum at concentration 1 M/L and in solvent DMF is observed in Fig. 7a, b. The calculated and experimental magnitudes of maximum wavelength (λ_{max}) are 372 nm (f = 0.23, Fig. 7a) and 375 nm (D = 2.106, Fig. 7b), respectively.

According to Table 11, the highest oscillations of the compound PAZB-12 observed at $\lambda_{max} =$ 344 nm and f = 0.33. Theoretical calculations show transitions [(H-4 → L), (H-2 → L), (H-1 → L + 1), (H → L)] are the most important Charge-Transfer in the compound PAZB-12 with absorption band at 344 nm (Fig. 8) that belong to the transition of one electron into the excited singlet state $S_0 \rightarrow S_3$. Excitation of one electron at 280 nm (f = 0.27) belonged to the transition into the state $S_0 \rightarrow S_8$ and describes by a wave function corresponding to a superposition of three configurations for one-electron excitations [(H-3 → L + 1), (H-1 → L + 1), (H → L + 2)]. The other excited states of the title compound have very small intensity (f ≈ 0) and are nearly forbidden by orbital symmetry considerations (Table 11).

The calculated UV/Vis spectrum of the compound PAZB-12 is obtained in solvent DMF (Fig. 9a) and experimental spectrum at concentration 0.2 M/L and in solvent DMF is observed in Fig. 9b. The calculated and experimental magnitudes of maximum wavelength (λ_{max}) are 344 nm (f = 0.33) and 377 nm (D = 0.920), respectively. Comparison of calculated and experimental absorption spectra of the compound PAZB-12 shows high accuracy of the constructed model calculations (Fig. 9a, b).

3.3. Frontier Molecular Orbital Analysis of the Compounds PAZB-3, PAZB-11, PAZB-12

Quantum chemical methods are important for obtaining information about molecular structure and electrochemical behavior of organic molecules. The frontier molecular orbitals (FMO) analysis plays an important role in the electronic and optical properties, UV/Vis spectrum and chemical reactions. The highest occupied molecular orbital (HOMO) can act as an electron donor and the lowest unoccupied molecular orbital (LUMO) can act as the electron acceptor. The high value of E_{HOMO} shows the tendency of the compound to donate electron to acceptor compound with low energy, whereas the low value of E_{LUMO} indicates that the compound accepts electrons. The FMO results of the title compounds such as electronic properties are summarized in Table 12.

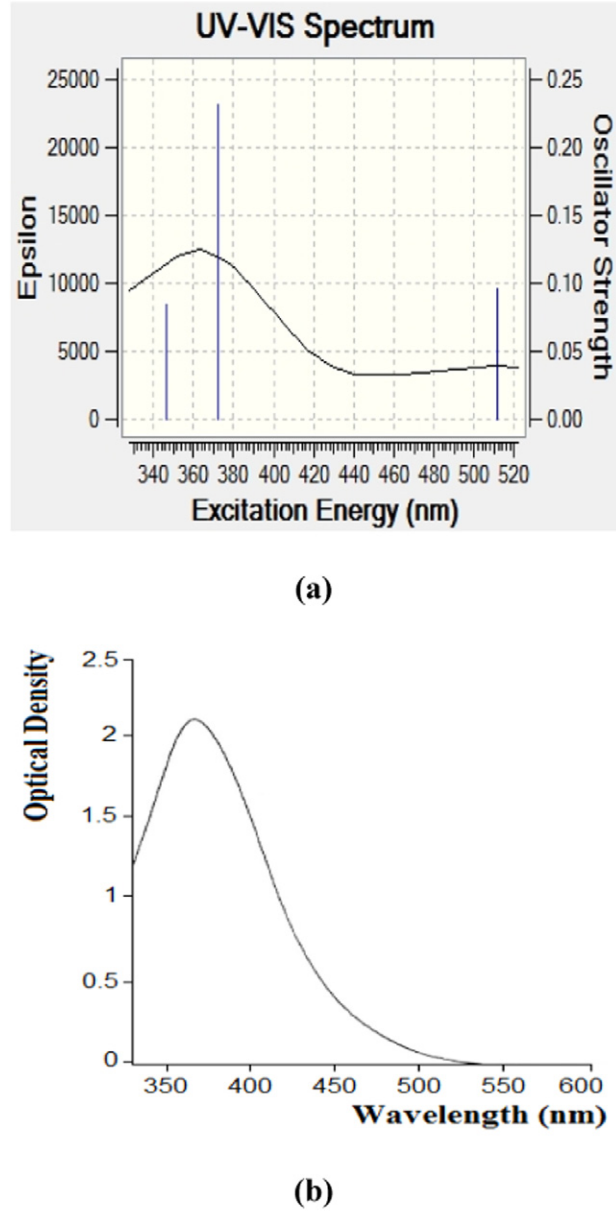

Fig. 7. UV/Vis spectrum of the compound PAZB-11 in solvent DMF: a) calculated by TDPBE1PBE/6-31 + G method and b) experimental at concentration of dye $3.6 \cdot 10^{-4}$ M.

Total electronic densities of states (DOSs) [16] of the compounds PAZB-3, PAZB-11, PAZB-12 were computed (Fig. 10). HOMO-LUMO energy gap is an important parameter in determining molecular electrical transport properties and reactivity of the molecules. Increase of the HOMO-LUMO energy gap decreases reactivity of the compound that lead to increase in the stability of the compound [27] (Fig. 10).

The DOS analysis indicates that the HOMO-LUMO energy gaps of the compounds PAZB-3, PAZB-11, PAZB-12 are about 3.69 eV, 3.69 eV and

Table 11
Electronic absorption spectrum of the compound PAZB-12 calculated by TDPBE1PBE/6-31G method.

Excited state	Wavelength (nm)	Excitation energy (eV)	Configurations composition (corresponding transition orbitals)	Oscillator strength (f)
S_1	513	2.41	−0.10(H-5 → L) + 0.29(H-2 → L) + 0.62(H → L)	0.07
S_2	362	3.42	−0.28(H-2 → L + 1) + 0.63(H → L + 1)	0.00
S_3	344	3.60	0.10(H-4 → L) + 0.58(H-2 → L) + 0.12(H-1 → L + 1) − 0.30(H → L)	0.33
S_4	329	3.76	0.69(H-1 → L)	0.00
S_5	297	4.16	−0.34(H-5 → L) + 0.52(H-4 → L) + 0.18(H-3 → L) − 0.16(H-2 → L)	0.03
S_6	288	4.29	−0.14(H-6 → L) + 0.51(H-5 → L) + 0.32(H-4 → L) − 0.11(H-1 → L + 1) − 0.24(H → L + 2)	0.03
S_7	281	4.40	0.10(H-7 → L + 1) + 0.61(H-2 → L + 1) + 0.29(H → L + 1)	0.00
S_8	280	4.41	−0.17(H-3 → L + 1) + 0.63(H-1 → L + 1) − 0.11(H → L + 2)	0.27
S_9	276	4.48	0.49(H-6 → L) + 0.22(H-5 → L) + 0.14(H-4 → L) + 0.33(H → L + 2) − 0.10(H → L + 3) + 0.12(H → L + 4) + 0.11(H → L + 5)	0.00
S_{10}	267	4.63	−0.15(H-4 → L) + 0.66(H-3 → L) + 0.14(H → L + 2)	0.00
S_{11}	261	4.74	−0.36(H-6 → L) + 0.19(H-9 → L) + 0.11(H-2 → L + 2) + 0.49(H → L + 2) + 0.17(H → L + 3)	0.12
S_{12}	254	4.86	−0.12(H-4 → L + 1) + 0.53(H-3 → L + 1) + 0.18(H-1 → L + 1) + 0.17(H-1 → L + 2) − 0.24(H-1 → L + 3) − 0.16(H-1 → L + 4)	0.18
S_{13}	246	5.02	0.23(H-6 → L) + 0.56(H → L + 3) − 0.12(H → L + 4) − 0.22(H → L + 5)	0.02
S_{14}	238	5.18	−0.32(H-6 → L + 1) − 0.10(H-5 → L+) + 0.53(H-4 → L + 1) + 0.12(H-3 → L + 1) + 0.23(H → L + 4)	0.01
S_{15}	237	5.21	0.10(H-6 → L + 1) − 0.19(H-4 → L + 1) + 0.14(H-2 → L + 2) + 0.18(H → L + 3) + 0.58(H → L + 4)	0.04
S_{16}	236	5.25	0.10(H-4 → L + 1) + 0.23(H → L + 3) + 0.59(H → L + 5)	0.04
S_{17}	230	5.37	0.60(H-2 → L) + 0.11(H-2 → L + 1) − 0.21(H-1 → L + 1) − 0.12(H → L + 1)	0.02
S_{18}	228	5.42	0.13(H-7 → L) − 0.14(H-3 → L + 1) + 0.20(H-2 → L + 2) + 0.61(H-1 → L + 2) + 0.10(H-1 → L + 5)	0.09
S_{19}	225	5.49	0.16(H-9 → L) + 0.61(H-7 → L) − 0.14(H-1 → L + 2) − 0.14(H → L + 6)	0.06
S_{20}	224	5.52	0.22(H-6 → L + 1) + 0.60(H-5 → L + 1) + 0.24(H-4 → L + 1)	0.00

H-HOMO, L-LUMO.

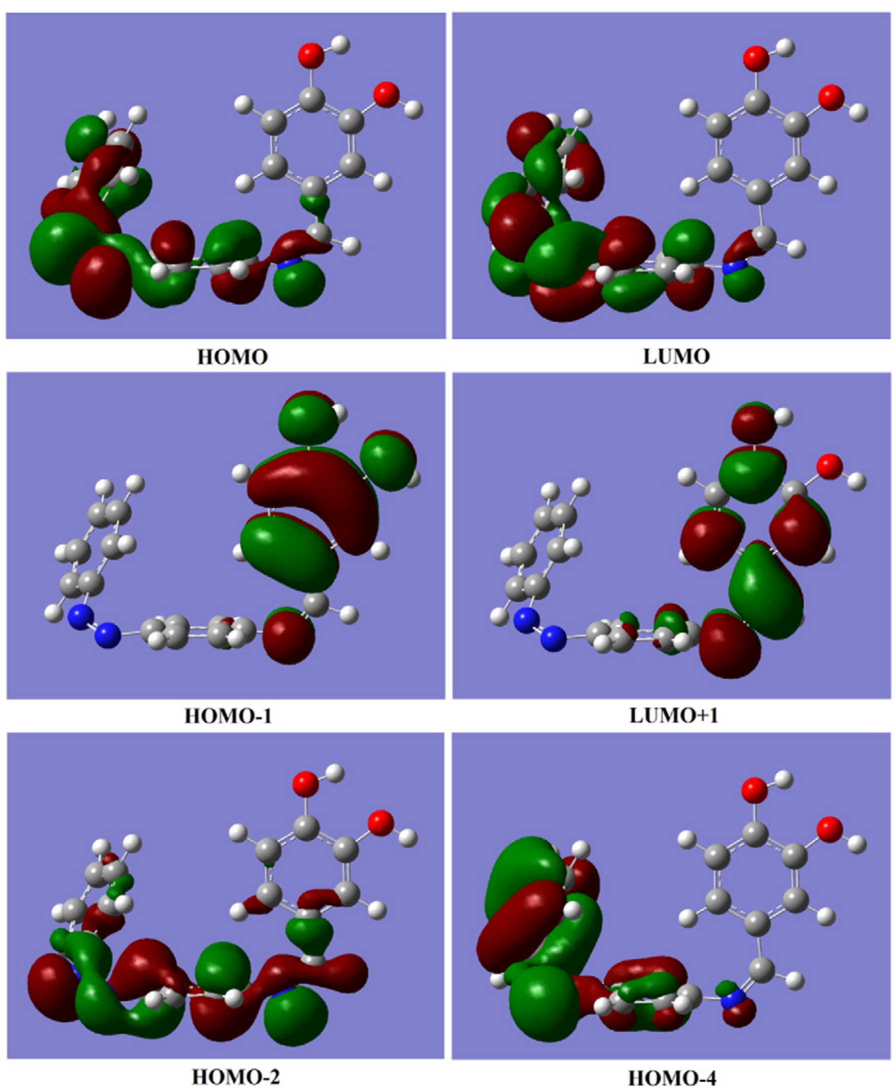

Fig. 8. Form of the MO involved in formation of absorption spectrum of the compound PAZB-12 at λ_{max} = 344 nm calculated by PBE1PBE/6-31G method.

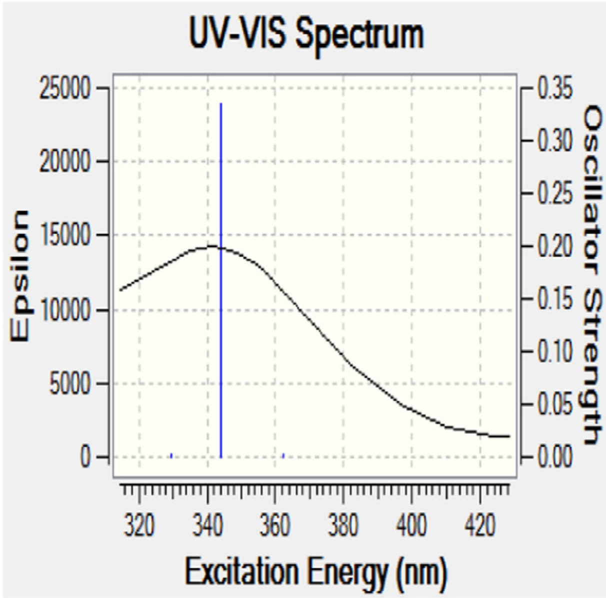

(a)

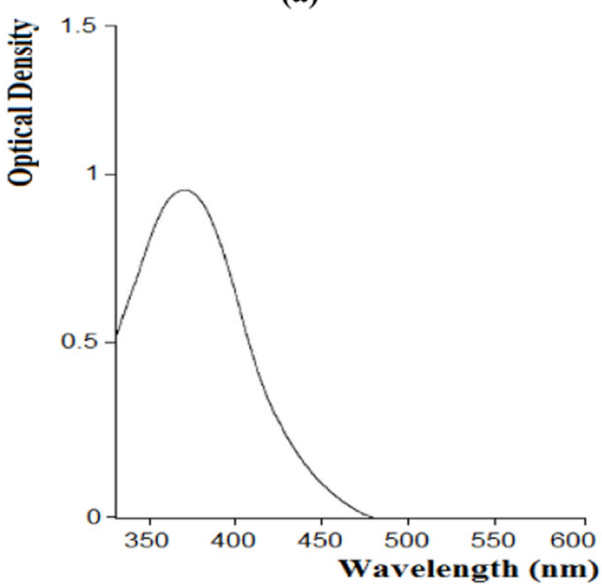

(b)

Fig. 9. UV/Vis spectrum of the PAZB-12 in solvent DMF: a) calculated by TDPBE1PBE/6-31G method and b) experimental at concentration of dye $2.7 \cdot 10^{-4}$ M.

Table 12
The calculated electronic properties of the title compounds using the PBE1PBE/6-31+G method.

Property	PAZB-3	PAZB-11	PAZB-12
E_{HOMO} (eV)	−6.16	−6.13	−6.16
E_{LUMO} (eV)	−2.47	−2.44	−2.42
Energy gap (eV)	3.69	3.69	3.74
Ionization potential I (eV)	6.16	6.13	6.16
Electron affinity A (eV)	2.47	2.44	2.42
Electronegativity (χ)	4.31	4.28	4.29
Global hardness (η)	1.84	1.84	1.87
Chemical potential (μ)	−4.31	−4.28	−4.29
Global electrophilicity (ω)	5.05	4.98	4.92
Chemical softness S (eV^{-1})	0.543	0.543	0.535
Dipole moment (Debye)	11.5439	11.6416	10.2798
Point group	C1	C1	C1

3.74 eV at the PBE1PBE/6-31+G method, respectively. The energy gap of the compound PAZB-12 has the highest value (3.74 eV) therefore it is less reactive compared with other structures. Therefore, the electronic transfer in the molecules PAZB-3, PAZB-11 is easier (Fig. 11).

The energy of HOMO is directly related to the ionization potential ($I = -E_{HOMO}$), while the energy of LUMO is related to the electron affinity ($A = -E_{LUMO}$). The global hardness ($\eta = I - A/2$), electronegativity ($\chi = I + A/2$), electronic chemical potential ($\mu = -(I + A)/2$) and electrophilicity ($\omega = \mu^2/2\eta$) [25], chemical softness ($S = 1/\eta$) [16] are calculated and is reported in Table 12. The global hardness (η) corresponds to the HOMO-LUMO energy gap. A molecule with a small energy gap has high chemical reactivity, low kinetic stability and is a soft molecule, while a hard molecule has a large energy gap [16]. The global hardness (η) of the compounds PAZB-3, PAZB-11, PAZB-12 is 1.84 eV, 1.84 eV and 1.87 eV respectively. From these values, we conclude that the compound PAZB-12 has the higher global hardness, therefore it is a hard molecule with high kinetic stability rather than the compounds PAZB-3, PAZB-11. Electronegativity (χ) is a measure of the power of an atom or a group of atoms to attract electrons and the chemical softness (S) describes the capacity of an atom or a group of atoms to receive electrons. The high values of dipole moment lead to stronger intermolecular interaction [25]. The dipole moment is a good measurement for the study of asymmetric nature of compounds. The magnitude of the dipole moment is related to the composition and dimensionality of the 3D compounds. All three compounds have relative high dipole moment values. The point group of the title compounds is C1, which refers to their high asymmetry. As can be seen from Table 12, the highest value of dipole moment is observed for the compound PAZB-11 (11.6416 Debye). On the other hands, the compound PAZB-11 is the most polar, whereas the compound PAZB-12 has the lowest polarity (10.2798 Debye). The high value of dipole moment for PAZB-11 is due to its asymmetric character. In the compound PAZB-11, the atoms are irregularly arranged which leads to the increasing dipole moment rather than other compounds.

3.4. Molecular Electrostatic Potential (MEP) of the Compounds PAZB-3, PAZB-11, PAZB-12

Molecular electrostatic potential (MEP) maps show the electronic density and are useful in recognition of sites of negative and positive electrostatic potentials for electrophilic attack and nucleophilic reactions as well as hydrogen bonding interactions [28,29]. The difference of the electrostatic potential at the surfaces is represented by different colors. The negative regions (red, orange and yellow color) of MEP with the high electron density were related to electrophilic reactivity, the positive regions (blue color) with the low electron density ones to nucleophilic reactivity and green color is neutral regions. The MEPs of the compounds PAZB-3, PAZB-11, PAZB-12 were obtained by theoretical calculations using the PBE1PBE/6-31+G level of energy (Fig. 12).

As shown in Fig. 12, the negative region (red color) of the compound PAZB-3 is mainly focused on N7, N8, N15 atoms. Therefore, these regions are suitable for electrophilic attack. The parts of the compound PAZB-3 are pale red such as phenyl rings that are sites with weak interaction. The hydrogen atom in O—H group (H39) of the compound PAZB-3 is positive potential site and it is suitable for nucleophilic activity (blue color), while the regions with pale blue color are sites with weak interaction. According to MEP maps of the compounds PAZB-11 andPAZB-12, the regions with pale blue are sites with weak interaction electrophilic attack. As can be seen from Fig. 12, the three hydrogen atoms such as H36, H37, H39 of the compound PAZB-11 and H37 of the compound PAZB-12 are the positive potential sites and these are suitable sites for nucleophilic activity (blue color). Also, the regions with green color of the three compounds indicate areas with zero potential (neutral sites).

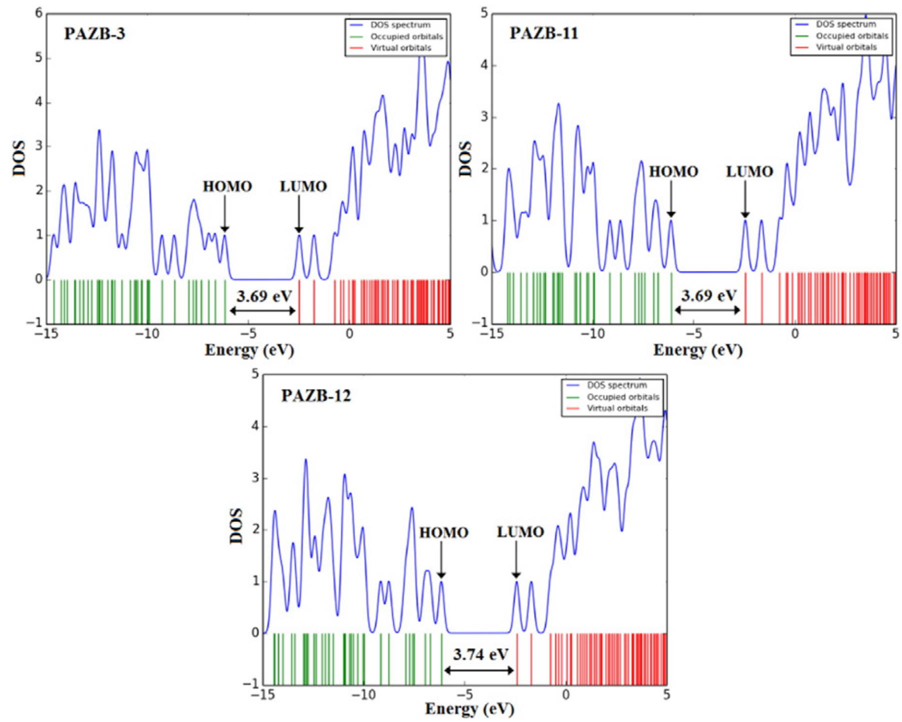

Fig. 10. Calculated DOS plots of the compounds PAZB-3, PAZB-11, PAZB-12 by PBE1PBE/6-31 + G method.

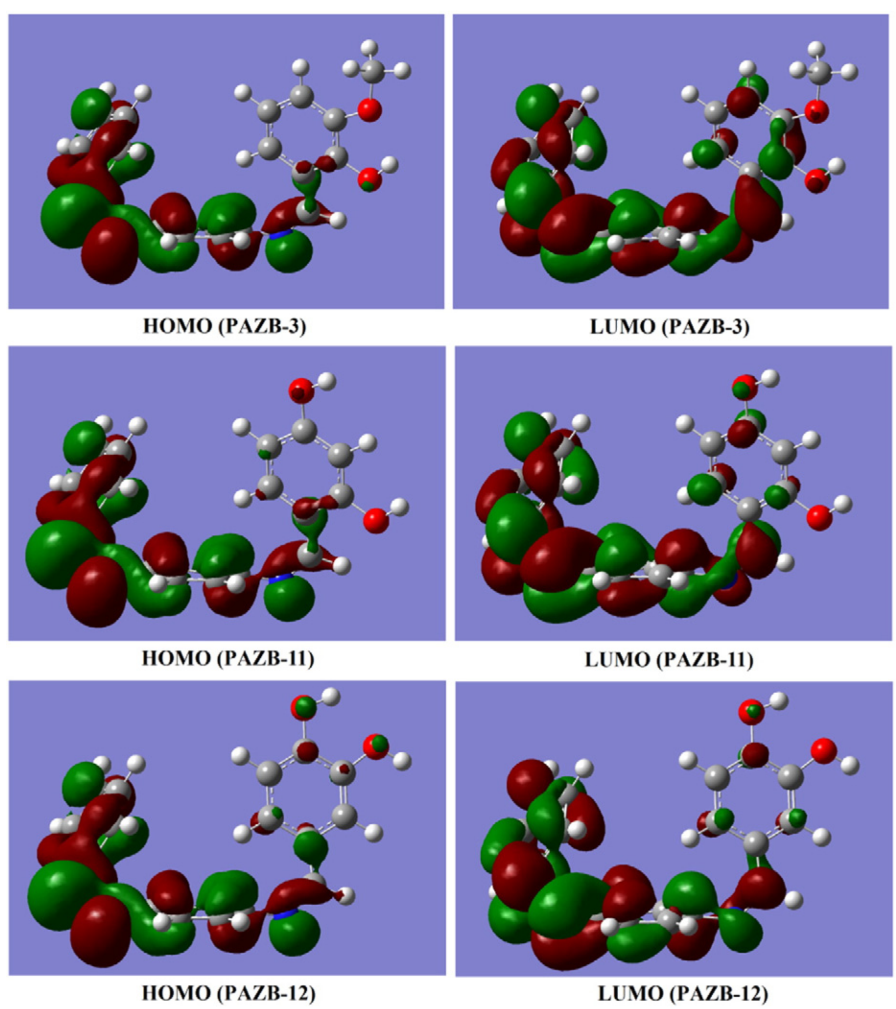

Fig. 11. Calculated Frontier molecular orbitals of the compounds PAZB-3, PAZB-11, PAZB-12by B3LYP/6-31 + G method.

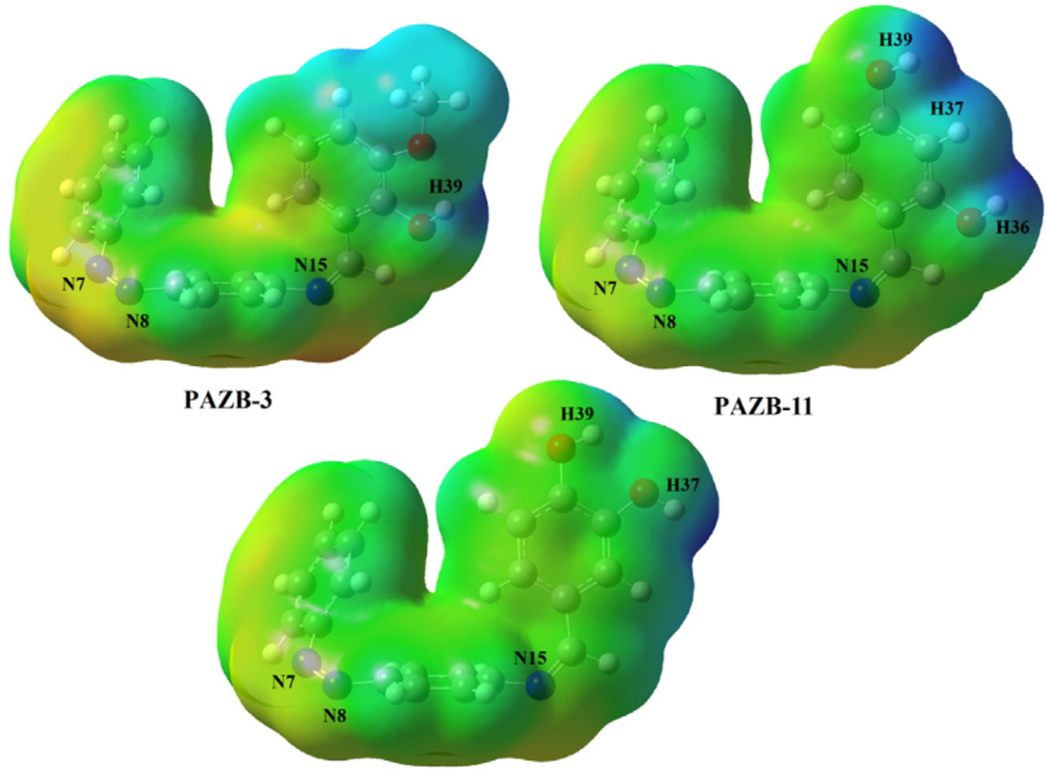

Fig. 12. Molecular electrostatic potential (MEP) map of the compounds PAZB-3, PAZB-11, PAZB-12 calculated using the PBE1PBE/6-31 + G level of energy

3.5. Natural Charge Analysis of the Compounds PAZB-3, PAZB-11, PAZB-12

The atomic charges play an important role on molecular polarizability, dipole moment, electronic structure and related properties of molecular systems [30]. We calculated the charge distributions for equilibrium geometry of the three compounds PAZB-3, PAZB-11, PAZB-12 by the NBO (natural charge) charges [25] using the PBE1PBE/6-31 + G level of energy. The calculated natural charges are listed in Table 13 (Atoms labeling is according to Fig. 3).

Based on these results, the total charge of the investigated compounds is equal to zero. Also Fig. 13 shows results of natural charges in graphical form. The natural charge (NBO) analysis of the title compounds show that carbon atoms have both positive and negative charges magnitudes. According to results in all three compounds, the positive carbons are observed for the carbon atoms attachment to the electron-withdrawing oxygen and nitrogen atoms. As can be seen from Table 13 and Fig. 13, the C6, C9, C12, C16, C20, C21 atoms in the compound PAZB-3, the C6, C9, C12, C16, C19, C20 atoms in the compound PAZB-11 and the C6, C9, C12, C16, C19, C20 atoms in the compound PAZB-12 have positive charge. The other carbon atoms of phenyl rings have negative charge. The oxygen and nitrogen atoms in all three structures have negative charge. As can be seen in Table 13 and Fig. 13, the negative charge of N15 atom in all three compounds is the higher than N7 and N8 atoms. The highest negative charge in the compounds PAZB-3, PAZB-11, PAZB-12 is observed for O23 atom (−0.726e), O23 atom (−0.725e) and O36 atom (−0.750e), respectively. According to Natural charge's plot all hydrogen atoms have the positive charge. In the three compounds, hydrogen atoms in the hydroxyl group have the highest positive charge compared with other hydrogen atoms due to the electron-withdrawing nature of the oxygen atoms, therefore they are acidic hydrogen atoms. Therefore, H39 atom (0.549e) in the compound PAZB-3, the H36 (0.543e) and H39 (0.539e) atoms in the compound PAZB-11 and the H37 (0.551e) and H39 (0.547e) atoms in the compound PAZB-12 are acidic hydrogen atoms.

3.6. NBO Analysis of the Compound PAZB-11

Natural bond orbital (NBO) analysis is important method for studying intra- and inter-molecular bonding and interaction between bonds in molecular systems [31]. Electron donor orbitals, acceptor orbitals and the interacting stabilization energy (E(2)) resulting from the second-order micro disturbance theory for the compound PAZB-11 are reported in Table 14.

The electron delocalization from filled NBOs (donors) to the empty NBOs (acceptors) describes a conjugative electron transfer process between them. For each donor (i) and acceptor (j), the stabilization energy E(2) associated with the delocalization i → j is estimated [30]:

$$E^{(2)} = \Delta E_{ij} = q_i \frac{F(i,j)^2}{\varepsilon_j - \varepsilon_i} \tag{3}$$

where q_i is the donor orbital occupancy, ε_j and ε_i are diagonal elements and F(i,j) is the off diagonal NBO Fock matrix element. The resonance energy (E(2)) detected the quantity of participation of electrons in the resonance between atoms. The larger E(2) value, the more intensive is the interaction between electron donors and acceptor, i.e. the more donation tendency from electron donors to electron acceptors and the greater the extent of conjugation of the whole system [31]. Delocalization of electron density between occupied Lewis-type (bond or lone pair) NBO orbitals and formally unoccupied (antibond or Rydberg) non Lewis NBO orbitals correspond to a stabilization donor–acceptor interaction. NBO analysis has been performed for the compound PAZB-11 the PBE1PBE/6-31 + G level of energy in order to elucidate the

Table 13
Natural charges (NBO charges, e) of the compounds PAZB-3, PAZB-11, PAZB-12 calculated using the PBE1PBE/6-31 + G level of energy.

PAZB-3		PAZB-11		PAZB-12	
Atoms	Natural charge	Atoms	Natural charge	Atoms	Natural charge
C1	−0.262	C1	−0.263	C1	−0.263
C2	−0.255	C2	−0.255	C2	−0.255
C3	−0.256	C3	−0.257	C3	−0.258
C4	−0.255	C4	−0.255	C4	−0.255
C5	−0.250	C5	−0.251	C5	−0.51
C6	0.041	C6	0.041	C6	0.041
N7	−0.171	N7	−0.173	N7	−0.174
N8	−0.156	N8	−0.157	N8	−0.157
C9	0.021	C9	0.018	C9	0.017
C10	−0.223	C10	−0.222	C10	−0.219
C11	−0.277	C11	−0.279	C11	−0.277
C12	0.118	C12	0.119	C12	0.122
C13	−0.267	C13	−0.270	C13	−0.276
C14	−0.240	C14	−0.240	C14	−0.238
N15	−0.245	N15	−0.456	N15	−0.447
C16	0.100	C16	0.098	C16	0.102
C17	−0.231	C17	−0.187	C17	−0.220
C18	−0.268	C18	−0.320	C18	−0.287
C19	−0.295	C19	0.325	C19	0.275
C20	0.242	C20	−0.385	C20	0.229
C21	0.297	C21	0.345	C21	−0.264
C22	−0.181	C22	−0.211	C22	−0.153
O23	−0.726	O23	−0.725	H23	0.277
O24	−0.563	H24	0.277	H24	0.274
C25	−0.391	H25	0.274	H25	0.272
H26	0.277	H26	0.272	H26	0.274
H27	0.274	H27	0.274	H27	0.276
H28	0.272	H28	0.276	H28	0.280
H29	0.274	H29	0.279	H29	0.278
H30	0.276	H30	0.277	H30	0.279
H31	0.280	H31	0.278	H31	0.280
H32	0.278	H32	0.280	H32	0.255
H33	0.279	H33	0.269	H33	0.276
H34	0.280	H34	0.278	H34	0.283
H35	0.269	H35	0.282	H35	0.278
H36	0.274	H36	0.543	O36	−0.750
H37	0.276	H37	0.279	H37	0.551
H38	0.280	O38	−0.720	O38	−0.721
H39	0.549	H39	0.539	H39	0.547
H40	0.268				
H41	0.244				
H42	0.244				

intramolecular, rehybridization and delocalization of electron density within the compound PAZB-11. The strong, moderate and weak intramolecular hyperconjugative interactions of the title compound such as $\pi \to \pi^*$, $\pi^* \to \pi^*$, $\sigma \to \sigma^*$, $n \to \sigma^*$ and $n \to \pi^*$ transitions are presented in Table 14. According to NBO analysis, the σ(C16-H33) → σ*(C12-N15) transition has the highest resonance energy (8.36 kcal/mol) compared with other $\sigma \to \sigma^*$ transitions of the title compound. The σ(C1-C2) orbital in phenyl ring participates as donor and the anti-bonding σ*(C1-C6), σ*(C2-C3) and σ*(C6-N7) orbitals act as acceptor with resonance energies (E(2)) of is 3.00 kcal/mol, 2.36 kcal/mol and 4.61 kcal/mol, respectively. These values indicate σ(C1-C2) → σ*(C6-N7) transition has the highest resonance energy (4.61 kcal/mol) compared with σ(C1-C2) → σ*(C1-C6) and σ(C1-C2) → σ*(C2-C3).

The intramolecular hyperconjugative interactions of the $\pi \to \pi^*$ transitions have the most resonance energy (E(2)) compared with $\sigma \to \sigma^*$ transitions. The important intramolecular hyperconjugative interaction of the $\pi \to \pi^*$ transitions in phenyl ring that lead to a strong delocalization are such as C11-C12 → C9-C10, C19-C20 → C21-C22 and C21-C22 → C17-C18 with the strong resonance energies (E(2)) 26.01 kcal/mol, 27.76 kcal/mol and 24.81 kcal/mol, respectively. The $\pi^* \to \pi^*$ transitions have the highest resonance energies compared with other interactions of the title compound. The highest resonance energy of the title compound is observed for C19-C20 → C17-C18, C21-C22 → N15-C16, C21-C22 → C17-C18 transitions with resonance energy (E(2)) 160.37 kcal/mol, 164.65 kcal/mol, 171.36 kcal/mol respectively, that lead to stability of the title compound. The strongest $n \to \sigma^*$ interactions are due to n2(O23) → π*(C16-H37) and n2(O38) → π*(C19-C20) interactions with stabilization energies of 29.04 kcal/mol and 30.87 kcal/mol, respectively.

The results of NBO analysis such as the occupation numbers with their energies for the interacting NBOs [interaction between natural bond orbital A and natural bond orbital B (A-B)] and the polarization coefficient amounts of atoms in the compound PAZB-11 are presented using the PBE1PBE/6–31 + G method is summarized in Table 15 (Atoms labeling is shown in Fig. 3).

The size of polarization coefficients shows the importance of the two hybrids in the formation of the bond in molecular system. The differences in electronegativity of the atoms involved in the bond formation are reflected in the larger differences in the polarization coefficients of the atoms (C—O, C—H C—N bonds). As can be seen from Table 15, the calculated bonding orbital for the σ(C19-O38) bond is the $\sigma = 0.5804(sp^{3.06}) + 0.8143(sp^{1.97})$ with high occupancy 1.99507 a.u. and low energy −0.95821 a.u. The polarization coefficients of C19 = 0.5804 and O38 = 0.8143 shows importance of O8 in forming σ(C19-O38) bond compared with C19 atom. The calculated bonding orbital for the π(N7-N8) bond is $\sigma = 0.7122(sp^{1.00}) + 0.7019\ (sp^{1.00})$ with high energy −0.40362 a.u. and high occupancy 1.95002 a.u. The polarization coefficients of N7 = 0.7122 and N8 = 0.7019 show low difference in polarization coefficients N7 and N8 atoms in N7-N8 bond and importance of two atoms in forming bond. According to NBO analysis, the natural hybrid orbital n1(O23) occupy a lower energy orbital (−0.61155 a.u) with p-character (56.77%) and high occupation number (1.97651 a.u), whereas n2(O23) with occupancy 1.87298 a.u. and high energy −0.35434 a.u. has p-character (100%). The pure p-type lone pair orbital n2(O23) participates the electron donation to π*(C21-C22) in the n2(O23) → π*(C21-C22) interaction with high resonance energies (E(2)) 29.04 kcal/mol in the title compound (see Table 14). The natural hybrid orbital n2(O38) with high occupancy 1.97911 a.u. and energy −0.60963 a.u. has p-character (100%). Therefore pure p-type lone pair orbital n2(O23) participates the electron donation to π*(C21-C22) in the n2(O23) → π*(C21-C22) interaction with high resonance energies (E(2)) 29.04 kcal/mol in the title compound. From Table 14, it is found that the p-type lone pair orbital n1(N15) participates the electron donation to π*(C19-C20) in the n2(O38) → π*(C19-C20) interaction with high resonance energies (E(2)) 30.87 kcal/mol.

3.7. Vibrational Frequencies of the Compounds PAZB-3, PAZB-11, PAZB-12

To confirm the accuracy of our findings, IR spectroscopy was used. Harmonic vibrational frequencies of the optimized compounds PAZB-3, PAZB-11, PAZB-12 were calculated using the PBE1PBE/6-31 + G method. The vibrational frequencies assignments were made using the GaussView05 program. The theoretical frequencies calculated by DFT method are usually higher than the corresponding experimental data due to the approximate treatment of the electron correlation, anharmonicity effects and basis set deficiencies [32]. The important calculated and experimental vibrational frequencies of compounds PAZB-3, PAZB-11, PAZB-12 are summarized in Tables 16, 17, 18, respectively. The fundamental vibrations appear in IR spectra of the azo compounds including azo group (N═N) stretching vibration in, C═N stretching mode, C—N stretching vibrations and C═C aromatic ring stretching vibrations. The azo group (N═N) stretching vibration in azo compounds shows important bands in the region 1400–1600 cm^{-1} [33]. The C—N stretching vibrations are expected in the range 1439–1306 cm^{-1} [34]. The C═N stretching mode in imines appears in the region 1690–1640 cm^{-1}. Also, the C═C aromatic ring stretching vibrations are expected in the range 1650–1200 cm^{-1} [35]. The C—H aromatic bending vibrations out of plane are appeared in the region 900–667 cm^{-1} [36].

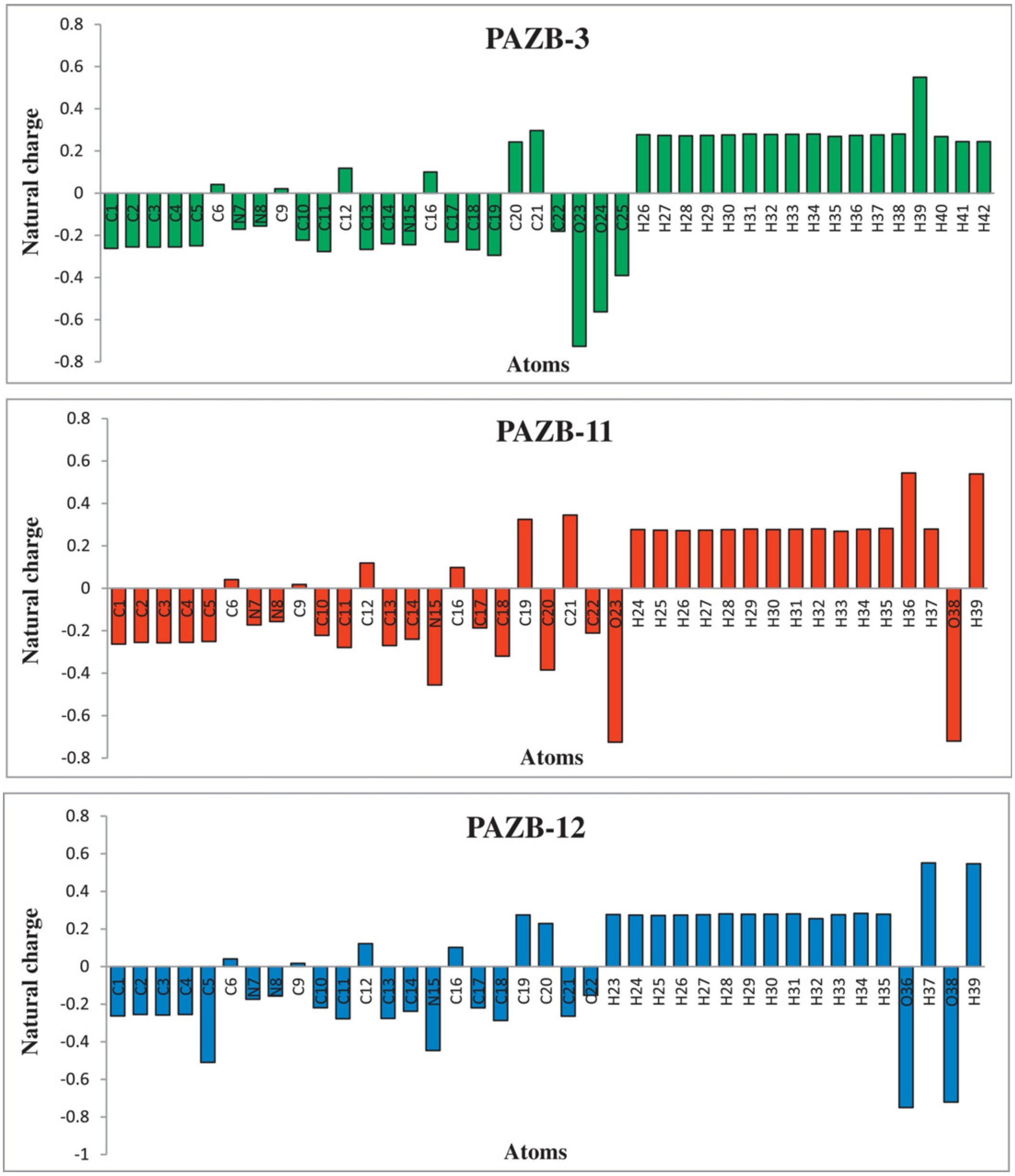

Fig. 13. Natural charges distribution of the compounds PAZB-3, PAZB-11, PAZB-12 calculated by PBE1PBE/6-31 + G method.

The symmetric C—H stretching vibrations of CH_3 are expected in the range 2900–3050 cm^{-1} [37,38]. Also, the C—O stretching vibration in ethers shows important bands in the region 1300–1050 cm^{-1} [39]. The experimental and calculated spectra of the title compounds are found to be in good agreement with each other. The important vibrational frequencies of the compound PAZB-3, PAZB-11, PAZB-12 are reported in the following:

3.7.1. PAZB-3

Based on our experimental results, we observe the C═N stretching vibration at 1614 cm^{-1} for the compound PAZB-3, while calculated value is predicted at 1721 cm^{-1}. Also, N═N stretching vibration is assigned at 1591 cm^{-1} and the corresponding theoretical value is 1666 cm^{-1}. The C—N stretching vibration is observed at 1440 cm^{-1}, whereas the DFT computation predicts this vibrational mode at 1459 cm^{-1}. The experimental and calculated values of C—O stretching vibration are assigned at 1259 cm^{-1} and 1276 cm^{-1}, respectively. The O—H stretching vibration that the experimental and calculated values are assigned at 3424 cm^{-1} and 3627 cm^{-1}, respectively. The symmetric and asymmetric C—H stretching vibrations of CH_3 are assigned at 2960 cm^{-1} and 3053 cm^{-1} and the corresponding theoretical values are 3076 cm^{-1} and 3168 cm^{-1}, respectively. These data indicate the presence of PAZB-3 (Table 16).

3.7.2. PAZB-11

In the compound PAZB-11, the experimental and theoretical C═N stretching vibrations is observed at 1637 cm^{-1} and 1717 cm^{-1}, respectively. The N═N stretching vibration is observed at 1491 cm^{-1}, whereas the DFT computation predicts this vibrational mode at 1548 cm^{-1}. Also, we observed experimental and calculated value of C—N stretching vibration at 1270 cm^{-1}. The C—O stretching vibration is assigned at 1295 cm^{-1} and the calculated value is predicted at 1338 cm^{-1}. The O—H stretching vibration that the experimental and calculated values are assigned at 3389 cm^{-1} and 3707 cm^{-1}, respectively. The

Table 14
Significant donor–acceptor interactions and second order perturbation energies of the compound PAZB-11 calculated using the PBE1PBE/6-31 + G level of energy.

Donor (i)	Occupancy	Acceptor (j)	Occupancy	E(2)[a] kcal/mol	E(j)–E(i)[b] a.u.	F(i, j)[c] a.u.
π(C1-C2)	1.67246	π*(C3-C4)	0.32897	21.15	0.29	0.070
		π*(C5-C6)	0.38502	21.92	0.29	0.072
π(C3-C4)	1.65333	π*(C1-C2)	0.31634	21.81	0.29	0.071
		π*(C5-C6)	0.38502	22.66	0.28	0.072
π(C5-C6)	1.64658	π*(C1-C2)	0.31634	20.61	0.30	0.071
		π*(C3-C4)	0.32897	20.65	0.30	0.071
π(C9-C10)	1.63102	π*(N7-N8)	0.17009	16.73	0.29	0.058
		π*(C11-C12)	0.39457	19.22	0.23	0.067
		π*(C13-C14)	0.30063	22.31	0.30	0.074
π(C11-C12)	1.61915	π*(C9-C10)	0.40634	26.01	0.29	0.078
		π*(C13-C14)	0.30063	18.10	0.29	0.067
π(C19-C20)	1.67248	π*(C21-C22)	0.45289	27.76	0.29	0.083
π(C21-C22)	1.61774	π*(N15-C16)	0.14344	20.05	0.29	0.073
		π*(C17-C18)	0.30039	24.81	0.30	0.079
π*(C19-C20)	0.39893	π*(C17-C18)	0.30039	160.37	0.02	0.084
π*(C21-C22)	0.45289	π*(N15-C16)	0.14344	164.65	0.01	0.069
		π*(C17-C18)	0.30039	171.36	0.02	0.082
σ(C1-C2)	1.97680	σ*(C1-C6)	0.02914	3.00	1.28	0.055
		σ*(C2-C3)	0.01626	2.36	1.30	0.050
		σ*(C6-N7)	0.05416	4.61	1.10	0.064
σ(C2-C3)	1.98067	σ*(C3-C4)	0.01624	2.22	1.30	0.048
σ(C3-C4)	1.98073	σ*(C2-C3)	0.01626	2.23	1.30	0.048
		σ*(C3-H26)	0.01163	1.09	1.21	0.033
σ(C4-C5)	1.97781	σ*(C6-N7)	0.05416	4.09	1.10	0.060
σ(C5-C6)	1.97205	σ*(C1-C6)	0.02914	3.80	1.29	0.063
		σ*(C6-N7)	0.05416	0.85	1.11	0.028
		σ*(N7-N8)	0.01468	2.17	1.26	0.047
σ(C9-C10)	1.97218	σ*(C9-C14)	0.03098	3.66	1.29	0.061
σ(C10-C11)	1.97548	σ*(C12-N15)	0.03088	4.27	1.17	0.063
σ(C10-H29)	1.97869	σ*(C9-C14)	0.03098	4.75	1.10	0.065
σ(C13-C14)	1.97431	σ*(N8-C9)	0.05228	4.78	1.11	0.066
σ(C16-H33)	1.97258	σ*(C12-N15)	0.03088	8.36	0.99	0.081
n1(N7)	1.90332	σ*(C1-C6)	0.02914	4.44	0.96	0.059
		π*(C5-C6)	0.38502	7.07	0.42	0.052
		σ*(N8-C9)	0.05228	13.98	0.78	0.094
n1(N8)	1.91195	σ*(C6-N7)	0.05416	14.30	0.77	0.095
		σ*(C9-C10)	0.02257	0.54	0.96	0.021
		π*(C9-C10)	0.40634	4.14	0.41	0.040
		σ*(C9-C14)	0.03098	6.42	0.96	0.071
n1(N15)	1.83305	σ*(C11-C12)	0.02949	2.55	0.89	0.044
		π*(C11-C12)	0.39457	18.18	0.36	0.076
		σ*(C16-C22)	0.04173	13.87	0.82	0.098
		σ*(C16-H33)	0.02192	3.81	0.81	0.052
n1(O23)	1.97651	σ*(C16-H33)	0.02192	0.92	1.08	0.028
		σ*(C20-C21)	0.02363	5.94	1.17	0.074
		σ*(C21-C22)	0.03059	0.71	1.15	0.026
n2(O23)	1.87298	π*(C21-C22)	0.45289	29.04	0.35	0.099
n1(O38)	1.97911	σ*(C18-C19)	0.02441	0.57	1.16	0.023
		σ*(C19-C20)	0.02654	6.45	1.16	0.077
n2(O38)	1.86825	π*(C19-C20)	0.39893	30.87	0.35	0.100

[a] E(2) Energy of hyper conjugative interactions.
[b] Energy difference between donor and acceptor i and j NBO orbitals.
[c] F(i, j) Is the Fock matrix element between i and j NBO orbitals.

asymmetric C—H aromatic stretching vibrations are assigned at 2923 cm^{-1}, 2853 cm^{-1} and the corresponding theoretical values are 3231 cm^{-1}, 3225 cm^{-1}, respectively. The presence of PAZB-11 is confirmed with these vibrational frequencies (Table 17).

3.7.3. PAZB-12

As can be seen Table 18, the experimental and calculated values of C═N stretching vibration of the compound PAZB-12 are assigned at 1644 cm^{-1} and 1733 cm^{-1}, respectively. Also, N═N stretching vibration is assigned at 1527 cm^{-1} and the corresponding theoretical value is 1550 cm^{-1}. The C—N stretching vibration is observed at 1518 cm^{-1}, whereas the calculated value predicts this vibrational mode at 1538 cm^{-1}. The other important vibration mode of the compound PAZB-12 is O—H stretching vibration that the experimental and calculated values are assigned at 3381 cm^{-1} and 3643 cm^{-1}, respectively. The experimental and calculated values of C—O stretching vibration are assigned at 1293 cm^{-1} and 1299 cm^{-1}, respectively. These vibrational modes indicate the presence of PAZB-12 (Table 18).

As seen in all four structures, the calculated values are in excellent agreement with experimental data.

4. Conclusion

Density functional theory (DFT/PBE1PBE/6-31 + G*) were modeled 3 new azomethine dyes absorbing in the ultraviolet region of spectrum. Their optimal geometries and absorption spectra in solvent DMF were calculated. These azomethine dyes were synthesized after spending quantum chemical studies. Based on PVA and the synthesized azomethine dyes were developed polarizing films operating at visible region of spectrum. Polarizing efficiency of colored oriented PVA-films

Table 15
Calculated natural bond orbitals (NBO) and the polarization coefficient for each hybrid in selected bonds of the compound PAZB-11 using the PBE1PBE/6-31+G level of energy.

Occupancy (a.u.)	Bond (A-B)[a]	Energy (a.u.)	ED_A (%)	ED_B (%)	NBO	S(%) (A)	S(%) (B)	P(%) (A)	P(%) (B)
1.97680	σ(C1-C2)	−0.73130	50.48	49.52	0.7105 ($sp^{1.81}$) + 0.7037 ($sp^{1.89}$)	35.64	34.64	64.36	65.36
1.97207	σ(C1-C6)	−0.27289	48.92	51.08	0.6994 ($sp^{1.98}$) + 0.7147 ($sp^{1.71}$)	33.53	36.85	66.47	63.15
1.98067	σ(C2-C3)	−0.72556	50.19	49.81	0.7084 ($sp^{1.87}$) + 0.7058 ($sp^{1.89}$)	34.83	34.56	65.17	65.44
1.98073	σ(C3-C4)	−0.72628	49.87	50.13	0.7062 ($sp^{1.89}$) + 0.7080 ($sp^{1.87}$)	34.64	34.83	65.36	65.17
1.65333	π(C3-C4)	−0.26909	50.07	49.93	0.7076 ($sp^{1.00}$) + 0.7066 ($sp^{1.00}$)	0.00	0.00	100	100
1.98633	σ(C6-N7)	−0.81369	41.66	58.34	0.6454 ($sp^{2.76}$) + 0.7638 ($sp^{2.05}$)	26.59	32.75	73.41	67.25
1.98977	σ(N7-N8)	−1.03827	49.94	50.06	0.7067 ($sp^{2.15}$) + 0.7075 ($sp^{2.15}$)	31.73	31.77	68.27	68.23
1.95002	π(N7-N8)	−0.40362	50.73	49.27	0.7122 ($sp^{1.00}$) + 0.7019 ($sp^{1.00}$)	0.01	0.01	99.99	99.99
1.98651	σ(N8-C9)	0.82349	58.42	41.58	0.7644 ($sp^{1.99}$) + 0.6448 ($sp^{2.68}$)	33.64	27.16	66.54	72.84
1.97218	σ(C9-C10)	−0.73499	51.01	48.99	0.7142 ($sp^{1.79}$) + 0.6999 ($sp^{1.95}$)	35.84	33.87	64.16	66.13
1.98218	σ(C12-N15)	−0.82541	41.38	58.62	0.6433 ($sp^{2.50}$) + 0.7657 ($sp^{1.95}$)	28.55	33.95	71.45	66.05
1.98802	σ(N15-C16)	−0.92922	59.63	40.37	0.7722 ($sp^{1.51}$) + 0.6354 ($sp^{2.02}$)	39.91	33.14	60.09	66.86
1.94398	π(N15-C16)	−0.35598	61.16	38.84	0.7821 ($sp^{99.99}$) + 0.6232 ($sp^{99.99}$)	0.36	0.21	99.64	99.79
1.97488	σ(C17-C18)	−0.74166	50.11	49.89	0.7079 ($sp^{1.81}$) + 0.7064 ($sp^{1.82}$)	35.59	35.46	64.41	64.54
1.99507	σ(C19-O38)	−0.95821	33.69	66.31	0.5804 ($sp^{3.06}$) + 0.8143 ($sp^{1.97}$)	24.65	33.67	75.35	66.33
1.99445	σ(C21-O23)	−0.95690	24.24	33.48	0.5808 ($sp^{3.12}$) + 0.8141 ($sp^{1.99}$)	24.24	33.48	75.76	66.52
1.97258	σ(C16-H33)	−0.54915	63.72	36.28	0.7983 ($sp^{2.28}$) + 0.6023 (s)	30.49	100	69.51	–
1.97706	σ(C17-H34)	−0.55224	63.94	36.06	0.7996 ($sp^{2.26}$) + 0.6005 (s)	30.69	100	69.31	–
1.97520	σ(C20-H37)	−0.56566	63.95	36.05	0.7997 ($sp^{2.18}$) + 0.6004 (s)	31.43	100	68.57	–
1.99006	σ(O23-H36)	−0.79499	77.39	22.61	0.8797 ($sp^{3.29}$) + 0.4756 (s)	23.29	100	76.71	–
1.98997	σ(O38-H39)	−0.79154	77.18	22.82	0.8785 ($sp^{2.29}$) + 0.4777 (s)	22.99	100	77.01	–
1.90332	n1(N7)	−0.40554	–	–	$sp^{1.81}$	35.53	–	64.47	–
1.91195	n1(N8)	−0.40430	–	–	$sp^{1.87}$	34.80	–	65.20	–
1.83305	n1(N15)	−0.34504	–	–	$sp^{2.87}$	25.85	–	74.15	–
1.97651	n1(O23)	−0.61155	–	–	$sp^{1.31}$	43.23	–	56.77	–
1.87298	n2(O23)	−0.35434	–	–	$sp^{1.00}$	0.00	–	100	–
1.97911	n1(O38)	−0.60963	–	–	$sp^{1.31}$	43.36	–	56.64	–
1.86825	n2(O38)	−0.35214	–	–	$sp^{1.00}$	0.00	–	100	–

[a] A–B is the bond between atom A and atom B. (A: natural bond orbital and the polarization coefficient of atom; A–B: natural bond orbital and the polarization coefficient of atom B).

depends on the concentration of the dyes and stretching degree of the films was found. Polarizing PVA-films containing the azomethine dyes: PAZB-3, PAZB-11 and PAZB-12 have PE ≥ 90% and high transmittance at concentration 0.3 wt% and $R_s = 3.5$. Stretched colored PVA-films by new synthesized structures have phenomenon of anisotropy of thermal and electrical conductivity. Thermal and electrical conductivity in a direction of orientation ($\lambda_{\|}$, $\delta_{\|}$) is higher than in a direction perpendicular orientations ($\lambda_{\perp}$, $\delta_{\perp}$). The manufactured polarizing PVA-films were used for optoelectronic applications and devices in Institute of Physical Organic Chemistry of the National Academy of Sciences of Belarus.

Appendix A. Supplementary data

Supplementary data to this article can be found online at https://doi.org/10.1016/j.saa.2017.11.029.

Table 16
Experimental and calculated vibrational frequencies and their assignment of compound PAZB-3 by using PBE1PBE/6-31+G method.

$\nu_{exp.}$ (cm^{-1})	$\nu_{cal.}$ (cm^{-1})	IR intensity	Assignment
560	612	13.08	C—H aromatic bending vibrations, out of plane
684	717	65.70	C—H aromatic bending vibrations, out of plane
738	765	30.91	C—H aromatic bending vibrations, out of plane
769	802	82.31	CvH aromatic bending vibrations, out of plane
847	895	128.92	C—H aromatic bending vibrations, out of plane
970	1005	22.90	C—H aromatic bending vibrations, out of plane
1137	1173	106.88	C—N stretching vibrations
1149	1197	143.38	C—N stretching vibrations, C—H aromatic bending vibrations
1197	1215	193	C—O stretching vibrations, O—H bending vibrations
1259	1276	13.65	C—O stretching vibrations, O—H bending vibrations
1440	1459	174.99	C—N stretching vibrations, C—H bending vibrations of N=C—H
1467	1492	29.38	C—H bending vibrations of CH_3
1569	1621	5.29	C=C aromatic stretching vibrations
1591	1666	214.01	N=N stretching vibrations, C=C aromatic stretching vibrations
1614	1721	531.65	C=N stretching vibrations
2960	3076	52.82	Symmetric C—H stretching vibrations of CH_3
3053	3168	31.24	Asymmetric C—H stretching vibrations of CH_3
3424	3627	254.97	O—H stretching vibration

Table 17
Experimental and calculated vibrational frequencies and their assignment of compound PAZB-11 by using PBE1PBE/6-31+G method.

$\nu_{exp.}$ (cm^{-1})	$\nu_{cal.}$ (cm^{-1})	IR intensity	Assignment
689	717	75.10	C—H aromatic bending vibrations, out of plane
764	788	78.74	C—H aromatic bending vibrations, out of plane
839	864	34.54	C—H aromatic bending vibrations, out of plane
977	999	37.05	C—H aromatic bending vibrations, out of plane
1134	1157	29.44	C—H aromatic bending vibrations
1154	1172	204.62	C—N stretching vibrations, C—H aromatic bending vibrations
1192	1216	0.25	C—H aromatic bending vibrations
1219	1236	18.66	C—H aromatic bending vibrations
1270	1270	2.05	C—N stretching vibrations, C—H aromatic bending vibrations
1295	1338	257.64	C—O stretching vibrations, O—H bending vibrations
1331	1359	1.23	C—H aromatic bending vibrations
1358	1373	90.99	C=C aromatic stretching vibrations, O—H bending vibrations
1440	1469	126.25	C—H bending vibrations of N=C—H
1458	1472	4.63	C=C aromatic ring stretching vibrations
1491	1548	375.36	N=N stretching vibrations
1573	1620	6.23	C=C aromatic ring stretching vibrations
1596	1662	234.47	C=C aromatic ring stretching vibrations, C=N stretching vibrations
1613	1664	394.56	N=N stretching vibrations, C=C aromatic ring stretching vibrations
1637	1717	441.78	C=N stretching vibrations, C=C aromatic ring stretching vibrations
2682	3205	17.75	C—H stretching vibration of N=C—H
2853	3225	2.2	Asymmetric C—H aromatic stretching vibrations
2923	3231	1.54	Asymmetric C—H aromatic stretching vibrations
3389	3707	162.95	O—H stretching vibration

Table 18
Experimental and calculated vibrational frequencies and their assignment of compound PAZB-12 by using PBE1PBE/6-31 + G method.

$\nu_{exp.}$ (cm^{-1})	$\nu_{cal.}$ (cm^{-1})	IR intensity	Assignment
683	717	81.93	C—H aromatic bending vibrations, out of plane
768	787	65.34	C—H aromatic bending vibrations, out of plane
813	817	55.57	C—H aromatic bending vibrations, out of plane
843	859	36.43	C—H aromatic bending vibrations, out of plane
1018	1021	3.58	C—H aromatic bending vibrations, out of plane
1147	1171	184.32	C—N stretching vibrations, C—H aromatic bending vibrations
1165	1197	126.76	C—N stretching vibrations, C—H aromatic bending vibrations
1190	1211	587.15	C—H aromatic bending vibrations, O—H bending vibrations
1293	1299	107.79	C—O stretching vibrations, C—H aromatic bending vibrations
1384	1396	0.60	C═C aromatic ring stretching vibrations
1441	1472	44.83	C═C aromatic ring stretching vibrations, C—H bending vibration of N═C—H
1518	1538	14.99	C—N stretching vibrations, C—H aromatic bending vibrations
1527	1550	420.23	N═N stretching vibrations
1568	1592	217.92	C═C aromatic ring stretching vibrations
1596	1621	11.15	C═C aromatic ring stretching vibrations
1644	1733	518.57	C═N stretching vibrations
2853	3159	74.18	C—H stretching vibrations of N═C—H
2923	3225	240	Asymmetric C—H aromatic stretching vibrations
3063	3226	11.04	Asymmetric C—H aromatic stretching vibrations
3381	3643	247.60	O—H stretching vibrations

References

[1] H. Zollinger, Color Chemistry: Synthesis, Properties, and Applications of Organic Dyes and Pigments, 2nd ed. VCH, Weinheim, 1991.
[2] R. Gup, E. Giziroglu, B. Kırkan, Dyes Pigments 73 (2007) 40, https://doi.org/10.1016/j.dyepig.2005.10.005.
[3] M. Gaber, T.A. Fayed, S. El-Daly, Y.S.Y. El-Sayed, Spectrochim. Acta A 68 (2007) 169, https://doi.org/10.1016/j.saa.2006.11.030.
[4] H.E. Katz, K.D. Singer, J.E. Sohn, C.W. Dirk, L.A. King, H.M. Gordon, J. Am. Chem. Soc. 109 (1987) 6561, https://doi.org/10.1021/ja00255a079.
[5] S.S. Kandil, Transit. Met. Chem. 23 (1998) 461.
[6] A. Bolduc, S. Dufresne, W.G. Skene, J. Mater. Chem. 22 (2012) 5053, https://doi.org/10.1039/C2JM14248A.
[7] M. Kurtoglu, N. Birbicer, U. Kimyonsen, S. Serin, Dyes Pigments 41 (1999) 143, https://doi.org/10.1016/S0143-7208(98)00077-1.
[8] A.A. Jarrahpour, M. Motamedifar, K. Pakshir, N. Hadi, M. Zarei, Molecules 9 (2004) 815, https://doi.org/10.3390/91000815.
[9] S. Shahab, M. Sheikhi, L. Filippovich, R. Kumar, E. Dikusar, H. Yahyaei, M. Khaleghian, J.Mol. Struct, 1148 (2017) 134, https://doi.org/10.1016/j.molstruc.2017.07.036.
[10] S. Shahab, R. Kumar, M. Darroudi, M.Y. Borzehandani, J. Mol. Struct. 1083 (2015) 198, https://doi.org/10.1016/j.molstruc.2014.11.064.
[11] A. Iwan, M. Palewicz, M. Krompiec, M. Grucela-Zajac, E. Schab-Balcerzak, A. Sikora, Mol. Biomol. Spectrosc. 97 (2012) 546, https://doi.org/10.1016/j.saa.2012.06.054.
[12] E.M. Nowak, J. Sanetra, M. Grucela, E. Schab-Balcerzak, Mater. Lett. 157 (2015) 93, https://doi.org/10.1016/j.matlet.2015.05.122.
[13] H. Almodarresiyeh, S. Shahab, V. Zelenkovsky, N. Ariko, L. Filippovich, V. Agabeko, J. Appl. Spectrosc. 81 (2014) 31, https://doi.org/10.1007/s10812-014-9882-0.
[14] H. Almodarresiyeh, S. Shahab, V. Zelenkovsky, V. Agabekov, J. Appl. Spectrosc. 81 (2014) 161 (0021-9037/14/8101-016).
[15] K. Fukui, Science 218 (1982) 747, https://doi.org/10.1126/science.218.4574.747.
[16] M. Sheikhi, D. Sheikh, Rev. Roum. Chim. 59 (2014) 761.
[17] P.G. Parr, W. Yang, J. Am. Chem. Soc. 106 (1984) 4049, https://doi.org/10.1021/ja00326a036.
[18] S. Shahab, L. Filippovich, R. Kumar, M. Darroudi, M. Yousefzadeh Borzehandani, M.J. Gomar, Mol. Struct. 1101 (2015) 109, https://doi.org/10.1016/j.molstruc.2015.08.007.
[19] S. Shahab, H. Alhosseini Almodarresiyeh, R. Kumar, M.J. Darroudi, Mol. Struct. 1088 (2015) 105, https://doi.org/10.1016/j.molstruc.2015.01.047.
[20] S. Shahab, R. Kumar, M. Darroudi, M.Y.J. Borzehandani, Mol. Struct. 1083 (2015) 198, https://doi.org/10.1016/j.molstruc.2014.11.064.
[21] S. Shahab, H. Almodarresiyeh, L. Filipovich, R. Kumar, M. Darroudi, F.J. Haji Hajikolaee, Mol. Struct. 1107 (2016) 19, https://doi.org/10.1016/j.molstruc.2015.11.024.
[22] M. Kose, N. Kurtoglu, O. Gumussu, M. Tutak, V. McKee, D. Karakas, M.J. Kurtoglu, Mol. Struct. 1053 (2013) 89, https://doi.org/10.1016/j.molstruc.2013.09.013.
[23] A. Iwan, E. Schab-Balcerzak, M. Grucela-Zajac, L.J. Skorka, Mol. Struct. 1058 (2014) 130, https://doi.org/10.1016/j.molstruc.2013.10.067.
[24] M.J. Frisch, G.W. Trucks, H.B. Schlegal, G.E. Scuseria, M.A. Robb, et al., Gaussian 09, Revision A.02, Gaussian Inc., Wallingford, CT, 2009.
[25] M. Sheikhi, D. Sheikh, A. Ramazani, S. Afr. J. Chem. 67 (2014) 151.
[26] A. Frisch, A.B. Nielson, A.J. Holder, GAUSSVIEW User Manual, Gaussian Inc., Pittsburgh, PA, 2000.
[27] A. Soltani, F. Ghari, A. DehnoKhalaji, E. TazikehLemeski, K. Fejfarova, M. Dusek, M. Shikhi, Mol. Biomol. Spectrosc. 139 (2015) 271, https://doi.org/10.1016/j.saa.2014.10.099.
[28] D. Habibi, A.R. Faraji, D. Sheikh, M. Sheikhi, S. Abedi, RSC Adv. 4 (2014) 47625, https://doi.org/10.1039/C4RA06463A.
[29] A. Ramazani, A. Rouhani, E. Mirhadi, M. Sheikhi, K. Ślepokura, T. Lis, Nano. Chem. Res. 1 (2016) 87–107, https://doi.org/10.7508/ncr.2016.01.011.
[30] S. Guidara, A.B. Ahmed, Y. Abid, H. Feki, Mol. Biomol. Spectrosc. 127 (2014) 275, https://doi.org/10.1016/j.saa.2014.02.028.
[31] F. Weinhold, C.R. Landis, Natural Bond Orbitals and Extensions of Localized, 2001.
[32] H. Tanak, J. Phys. Chem. A 115 (2011) 5133, https://doi.org/10.1021/jp104752k.
[33] B.L. Haymore, J.A. Ibers, D.W. Meek, Inorg. Chem. 14 (1975) 541, https://doi.org/10.1021/ic50145a018.
[34] R. Ramasamy, V. Krishnakumar, Spectrochim. Acta A 69 (2008) 8, https://doi.org/10.1016/j.saa.2007.02.020.
[35] L.J. Bellamy, The Infrared Spectra of Complex Molecules, 3rd ed. Wiley, New York, 1975.
[36] G. Varasanyi, Assignments for Vibrational Spectra of Seven Hundred Benzene Derivatives, I and II, Academic Kiaclo, Budapest, 1973.
[37] N.P.G.A. Roeges, Guide to Complete Interpretation of Infrared Spectra of Organic Structures, Wiley, New York, 1994.
[38] N.B. Colthup, L.H. Daly, S.E. Wiberly, Introduction to Infrared and Raman Spectroscopy, Academic Press, New York, 1975.
[39] Y.R. Sharma, Elementary Organic Spectroscopy, Principles and Applications, S. Chand & Company Ltd., 2007.